China Geology 7 (2024) 714−729

China Geology

Journal homepage: http://chinageology.cgs.cn
https://www.sciencedirect.com/journal/china-geology

Metallogenic characteristics of Shitoukengde intrusion and its implications for Ni-Co-(Cu) sulfide mineralization in East Kunlun

Xue-peng Duan[a, b,*], Fan-cong Meng[c], Zong-qi Wang[a], Xiao-fei Yu[a]

[a] *Development and Research Center, China Geological Survey, Ministry of Natural Resources, Beijing* 100037, *China*
[b] *China University of Geosciences (Beijing), Beijing* 100083, *China*
[c] *Key Laboratory of Deep-Earth Dynamics of Ministry of Natural Resources, Institute of Geology, Chinese Academy of Geological Sciences, Beijing* 100037, *China*

ARTICLE INFO

Article history:
Received 27 October 2022
Received in revised form 20 April 2023
Accepted 30 May 2023
Available online 10 October 2023

Keywords:
Troctolite
Zircon U-Pb
Mafic-ultramafic intrusion
Depleted asthenospheric mantle
Cu-Ni sulfide mineralization
East Kunlun orogenic belt
Shitoukengde

ABSTRACT

Xiarihamu deposit is the only super-large Ni-Co deposit found in East Kunlun orogenic belt (EKOB) until present. Shitoukengde (STKD) intrusion is considered to have the potential to become a large Ni-Co deposit in East Kunlun. In order to discuss the metallogenic potential, this study present petrographical, geochemical data, and zircon U-Pb dating for the STKD intrusion. The STKD intrusion is hosted within mafic-ultramafic rocks which contain peridotite, pyroxenite and gabbro, and mainly intruded into the marble of the Paleoproterozoic Jinshuikou Group. Harzburgite and orthopyroxenite are the main country rocks for the Cu-Ni sulfide mineralization. Combine with the positive $\varepsilon_{Hf}(t)$ values (+1.1 to +8.6) of zircons, the enrichment of LILEs, depletion of HFSEs, and lower Ce/Pb ratios of whole rocks indicate that the parental magma was originated from the depleted asthenospheric mantle and experienced 5%–15% crustal contamination. Troctolite formed during the Early Devonian and it has weighted mean $^{206}Pb/^{238}U$ age of 412 Ma. Regional background information has indicated that the post-collisional extension setting has already existed during the Early Devonian, leading to the formation of STKD intrusion and Cu-Ni sulfide mineralization. STKD intrusion may have the potential to be one economic Cu-Ni sulfide deposit but seems unlikely to be a super-large one.

1. Introduction

Mafic-ultramafic rocks have metallogenic specialization for magmatic Ni-Co-(Cu) sulfide deposits and may develop in different tectonic settings. It is well known that the continental rift, especially under the setting of the mantle plume, is the most favorable tectonic setting for the formation of super-large magmatic sulfide Cu-Ni-PGE deposits, such as Noril`sk-Talnakh from Russia (Naldrett AJ, 1997), Voisey`s Bay from Canada (Naldrett AJ, 1997; Li CS et al., 2001) and Jinchuan from China (Chai G and Naldrett AJ, 1992). However, the discovery of magmatic Ni-Co-(Cu) sulfide deposits in the East Kunlun orogenic belt (EKOB), including the Binggounan, Yugusayi, Akechukesai, Shitoukengde (STKD) Ni-Co-(Cu) occurrence, and the Xiarihamu (XRHM) world-class Ni-Co ore deposit, not only changes the distribution of magmatic Ni-Co-(Cu) deposit in China, but also indicates the metallogenic potential in the orogenic belt (Wang G et al., 2014; Jiang CY et al., 2015; Li CS et al., 2015; Peng B et al., 2016; Song XY et al., 2016; Liu YG et al., 2018; Song XY et al., 2020; Chen LM et al., 2021; He HL et al., 2022; Yang HH et al., 2022). There have been some studies on the tectonic setting of Ni-Cu deposits in the orogenic belt. Although most of the large Ni-Cu sulfide deposits in the southern margin of the Central Asian orogenic belt (CAOB) have a similar time of magmatic activity with that of the Tarim mantle plume, the ages of some other similar deposits and ore-bearing rock bodies in Gansu (Heishan, 365 Ma, Xie W et al., 2012) and Jilin (Hongqiling, 217 Ma, Wei B et al., 2013) are not the same. The geologic and geochemical characteristics of the XRHM intrusion in the western part of the EKOB indicate that the potential Ni reserves of the deposits in the EKOB can be more than 1 Mt of contained metal (Song XY et al., 2016). However, the tectonic setting of Ni-Co-(Cu) deposit in EKOB is still controversial, and there are at least four main ideas: (1) Subduction-related

* Corresponding author: *E-mail address*: duanxuepeng@yeah.net (Xue-peng Duan).

Literary editor: Li-qiong Jia
doi:10.31035/cg2023070
2096-5192/© 2024 China Geology Editorial Office.

extensional island arc (Jiang CY et al., 2015), (2) subduction-related Alaska-type setting (Li CS et al., 2015), (3) post-collision-related setting (Wang G et al., 2014; Song XY et al., 2016), (4) rift-related setting (Li WY et al., 2021, 2022). The determination of the tectonic setting affects the direction of regional prospecting. Therefore, the precise constraints of the tectonic setting are worthy of discussion.

The STKD Ni-Co-(Cu) ore occurrence was found by 108 Geological Brigade of Sichuan Bureau of Geology and Mineral Resources in 2013 during the ore exploration program. STKD mafic-ultramafic intrusion in the middle part of the EKOB is supposed to be in line with the characteristics of XRHM intrusion and has great potential for metallogenic (Zhou W et al., 2016). The initial exploration results show that the amount of Ni resources from disseminated sulfide ores is 68942.56 t with Ni grades ranging from 0.21% to 1.49%[①], less than a resource of ca. 1.6 Mt sulfide ores with average of 0.65% Ni in XRHM (Song XY et al., 2016). In this paper, mineral chemistry, whole-rock geochemistry, zircon U-Pb isotope and Hf isotope data are reported for the ore-bearing mafic-ultramafic rocks of STKD, to discuss the petrogenesis and the tectonic setting of the intrusion. Compared with the XRHM intrusion, we aim to provide some effective prospecting criteria for magmatic Ni-Co-(Cu) deposits in the EKOB.

2. Geological setting

At the northeastern margin of the Qinghai-Tibet plateau, the E-W-trending EKOB is positioned between the Qaidam block to the north and the Bayan Har-Songpan-Ganzi terrane to the south (Fig. 1). It is bordered to the west by the NE-SW trending Altyn sinistral strike-slip fault and to the northeast by the 1500 km long and 50–200 km wide Qinling orogenic belt. EKOB can be separated into two tectonic zones, the North East Kunlun Terrane (NEKT) and the South East Kunlun Terrane, using the Central East Kunlun Fault (CEKF) belt as the dividing line (Wu GJ et al., 1989; Xu ZQ et al., 2001; Xu ZQ et al., 2006).

The NEKT is characterized by extensive Meso- and Neoproterozoic metamorphic basements of the Jinshuikou Group and a series of large Paleozoic and Mesozoic granitic plutons. The Jinshuikou Group is mostly composed of gneiss, schist and marble, which was intruded by Neoproterozoic granites (Chen NS et al., 2006; Meng FC et al., 2013a), and underwent the Early Paleozoic amphibolite–granulite facies metamorphism (Wang YS et al., 1987; Wang GC et al., 2003; Wang GC et al., 2004a; Liu YJ et al., 2005; Chen NS et al., 2006; Chen NS et al., 2007; Wang GC et al., 2007). Recently, a zircon U-Pb geochronologic study of paragneiss and schist in the Jinshuikou Group suggests a Neoproterozoic metamorphic event (He DF et al., 2015). A zone of mafic-ultramafic intrusive rocks and ophiolite fragments occurs as tectonic lenses in a high-grade metamorphic complex containing eclogite along the CEKF (Yang JS et al., 1996; Meng FC et al., 2013b). Some researchers consider mafic-ultramafic intrusive rocks and the presence of eclogite-bearing metamorphic rocks as indicative of the presence of an early Paleozoic suture in the EKOB (Yang JS et al., 1996; Meng FC et al., 2013b; Meng FC et al., 2015a; Meng FC et al., 2015b). The Proterozoic metamorphic basement is overlain by

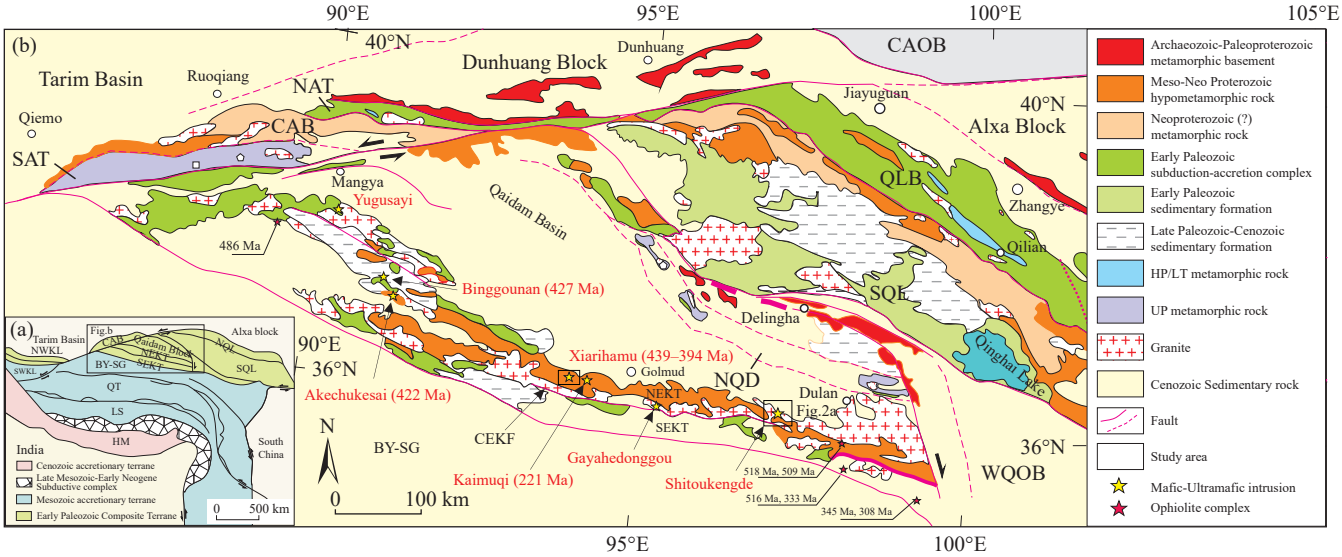

Fig. 1. Geological sketch map of the Altyn–Qilian–North Qaidam orogenic system in the northern Qinghai-Tibet Plateau (modified from Zhang JX et al., 2015). CAOB–Central Asian Orogenic Belt; NQL–North Qilian subduction-accretion complex belt; QLB–Qilian Block; NQD–North Qaidam subduction-collision complex; WQOB–West Qingling Orogenic Belt; NAT–North Altyn subduction-accretion complex belt; CAB–Central Altyn Block; SAT–South Altyn subduction-collision complex; NEKT–North East Kunlun Terrane; CEKF–Central East Kunlun Fault; SEKT–South East Kunlun Terrane; BY-SG–Bayan Har-Songpan-Ganzi Terrane; QT–Qiangtang Terrane; LS–Lhasa Terrane; HM–Himalaya Terrane; SWKT–South West Kunlun Terrane; NWKT–North West Kunlun Terrane.

[①]108 Geological Brigade of Sichuan Bureau of Geology and Mineral Resources. A summary report of Ni-Cu ore exploration in Dulan County, Qinghai Province in 2015. 2015.

low-grade metamorphosed Ordovician clastic rocks. The Ordovician strata are unconformably overlain by terrestrial volcanics of the Early Devonian Maoniushan Formation, which includes andesite, dacite, and rhyolite with basaltic interlayers (Lu L et al., 2010; Zhang YL et al., 2010). The Maoniushan Formation formed unconformably under the Carboniferous and Permian sedimentary and volcanic layers. Giant Paleozoic granitoid plutons were deposited in the Proterozoic metamorphic rocks and the late Ordovician strata in the NEKT (Mo XX et al., 2007). The zircon U-Pb ages (420–390 Ma) indicate that the Paleozoic granitoid plutons cover about 50% of the area in the eastern part of the NEKT and were mainly intercalated from Silurian to Early Devonian (Liu B et al., 2012, 2013b). In the western portion of the NEKT, the Paleozoic granitoid plutons formed slightly earlier and have been dated at 440–400 Ma (Zhao ZM et al., 2008). Another peak age of granitic magmatism related to the evolution of the Paleo-Tethys Ocean in the NEKT is 240–260 Ma, consistent with the findings in Triassic volcanism (Huang H et al., 2014; Ma CQ et al., 2015; Shao FL et al., 2017; Xia R et al., 2017). Although the exact timing of Paleo-Tethys closure is debated, the widespread igneous rocks in the NEKT suggest that strong reworking occurred during the formation of the Indochina orogeny (Mo XX et al., 2007; Xu ZQ et al., 2007).

The SEKT is composed of the Proterozoic Kuhai Group and the Wanbaogou Group, the early Paleozoic Naij Tai Group and the Late Devonian molasse formation (Jiang CF et al., 1992). The Kuhai Group is the oldest metamorphosed basement in the SEKT and is composed of felsic gneiss, amphibolite and marble (Wang GC et al., 2007; He DF et al., 2015; Liu Q et al., 2016). Different from the Jinshuikou Group, the protoliths (including clastic sediments, intermediate to basic volcanic carbonate rocks) of Kuhai Group merely experienced early Paleozoic amphibolite facies metamorphism (Liu YJ et al., 2005). Recently some researchers note that the basement in SEKT has a similar rock suit and experienced approximative contemporaneous metamorphism (423 Ma) to the basement in NEKT, indicating that they might have had similar sources and evolution histories (Liu Q et al., 2016). Some researchers suggested that the Wanbaogou Group comprising clastic sediments, marble and volcanic rocks may be the metamorphosed basement of SEKT and underwent green-schist facies metamorphism (Jiang CF et al., 1992; Pan YS et al., 1996). The Naij Tal Group contains a small number of fragments of early Paleozoic ophiolites such as Qushiang, Qingshuiquan and Wutuo that have undergone low-grade metamorphism (Yang JS et al., 1996; Zhu YH et al., 1999; Bian QT et al., 2004; Feng JY et al., 2010; Li RB et al., 2019, 2021). The late Devonian molasse formation marks the end of the early Paleozoic orogeny.

3. Petrography of the STKD intrusion

The STKD intrusion is about 2.5 km long and 1.5 km wide with an exposed area of about 4 km^2 (Fig. 2a). The

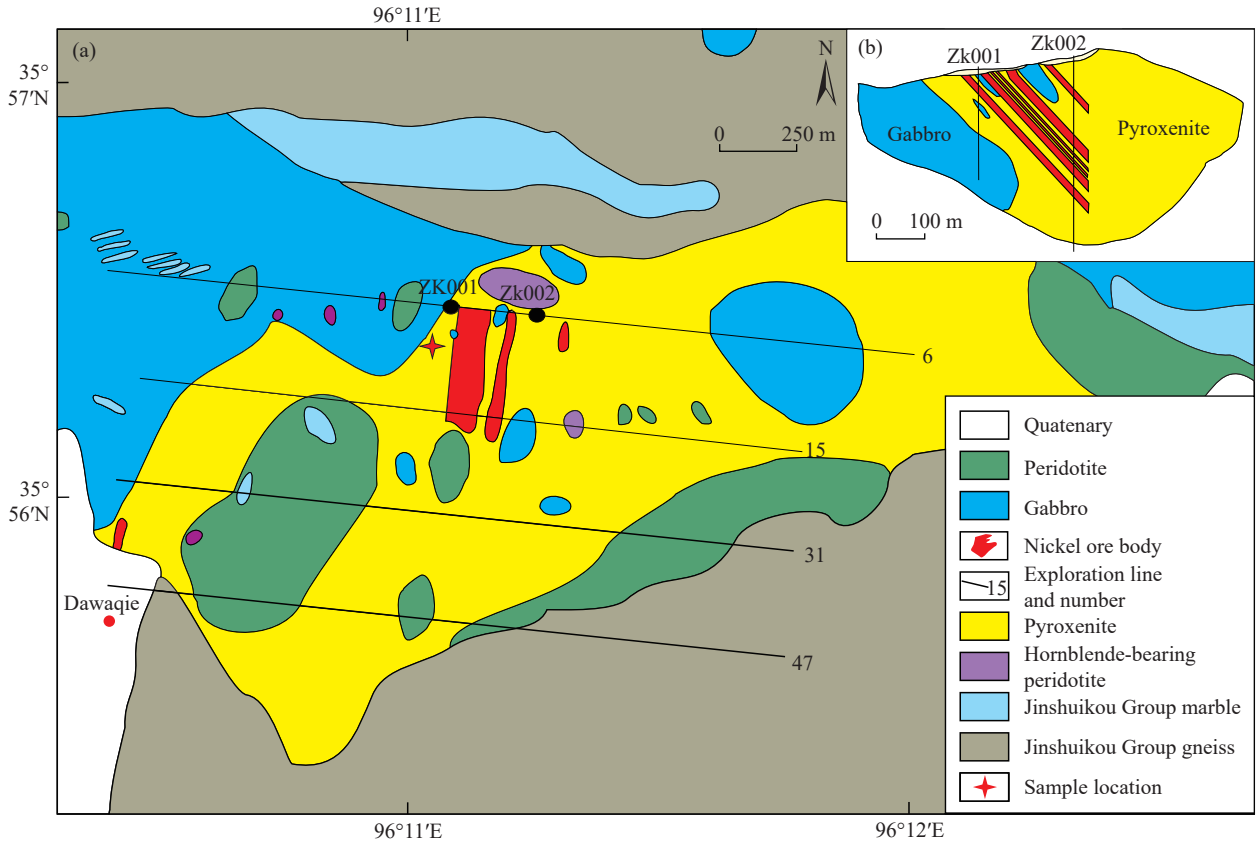

Fig. 2. a–Sketch geological map of the STKD intrusion (modified from Zhou W et al., 2016); b–map and cross sections of the STKD intrusion.

intrusions were emplaced in the metamorphic rocks of the Paleoproterozoic Jinshuikou Group and are dominantly in contact with marble (Fig. 3). Drill holes reveal that the intrusions strike approximately NW-SE and are mainly composed of peridotite, pyroxenite and gabbro (Fig. 2b). The order of emplacement is from gabbro to pyroxenite to peridotite. The contact between these portions is gradational and the ultramafic intrusions (including orthopyroxenite and harzburgite) are the main country rock of the Ni-Cu ores (exploration line 6 to 15). Ni-Cu ore body generally dip to the east at 20°–30°.

The ultramafic portion in the STKD intrusion mainly comprises dunite, harzburgite, wehrlite, Ol-clinopyroxenite, orthopyroxenite and websterite. Harzburgites are of great proportion and belong to peridotite; Ol-clinopyroxenite and orthopyroxenite belong to pyroxenite. Harzburgite (Fig. 4a) is represented by fine-to-medium grained (1.5–4.5 mm) cumulates and consists of 70% olivine, 20% orthopyroxene, minor clinopyroxene and sulfide. Olivine with stockwork serpentine and part of orthopyroxene are cumulates and interstitial minerals include orthopyroxene, clinopyroxene and sulfide. Orthopyroxenite (Fig. 4b) consists of 90% cumulus orthopyroxene and 10% intercumulus plagioclase. In addition, another sulfide-mineralized orthopyroxenite sample (Fig. 4c) contains 40% orthopyroxene and 60% sulfide (pentlandite and pyrrhotite form sideronitic texture).

The gabbroic portion is composed of troctolite and Ol-gabbro. The troctolite contains 40% euhedral olivine grains (Figs. 4d, e), with orthopyroxene zonal texture ranging in size from 0.5–1.5 mm with minor speckled sulfides, and 45% anhedral plagioclase fills in the interstitial spaces, and 15% euhedral spinel grains (2 mm) occur as oikocrysts growing closed to olivine grains. The Ol-gabbro is composed of clinopyroxene, plagioclase and minor olivine (Fig. 4f). The clinopyroxene grains range in size from 1–2 mm with modal content of about 45%. The plagioclase constitutes 45% and ranges in size from 1.5–2.5 mm.

Part of early-crystallized minerals experienced variable degrees of hydrothermal alteration along fractures. It potentially increases the volatile contents and changes the fluid compositions during the late stages of magmatism or the post-magmatic stage. The olivine shows partially altered to serpentine; Orthopyroxene is variably replaced by talc; Clinopyroxene is partially altered to actinolite; Plagioclase is partially replaced by albite.

4. Analytical methods

4.1. Mineral chemistry

Mineral chemical compositions were obtained at the State Key Laboratory for Continental Tectonics and Dynamics, Institute of Geology, Chinese Academy of Geological Sciences (CAGS), Beijing, China, using a JXA-8100 electron probe micro analyzer (EPMA) with an accelerating voltage of 20 keV, a beam current 20 nA, and beam diameters of 5 μm, and a 10–30 s counting time on a peak.

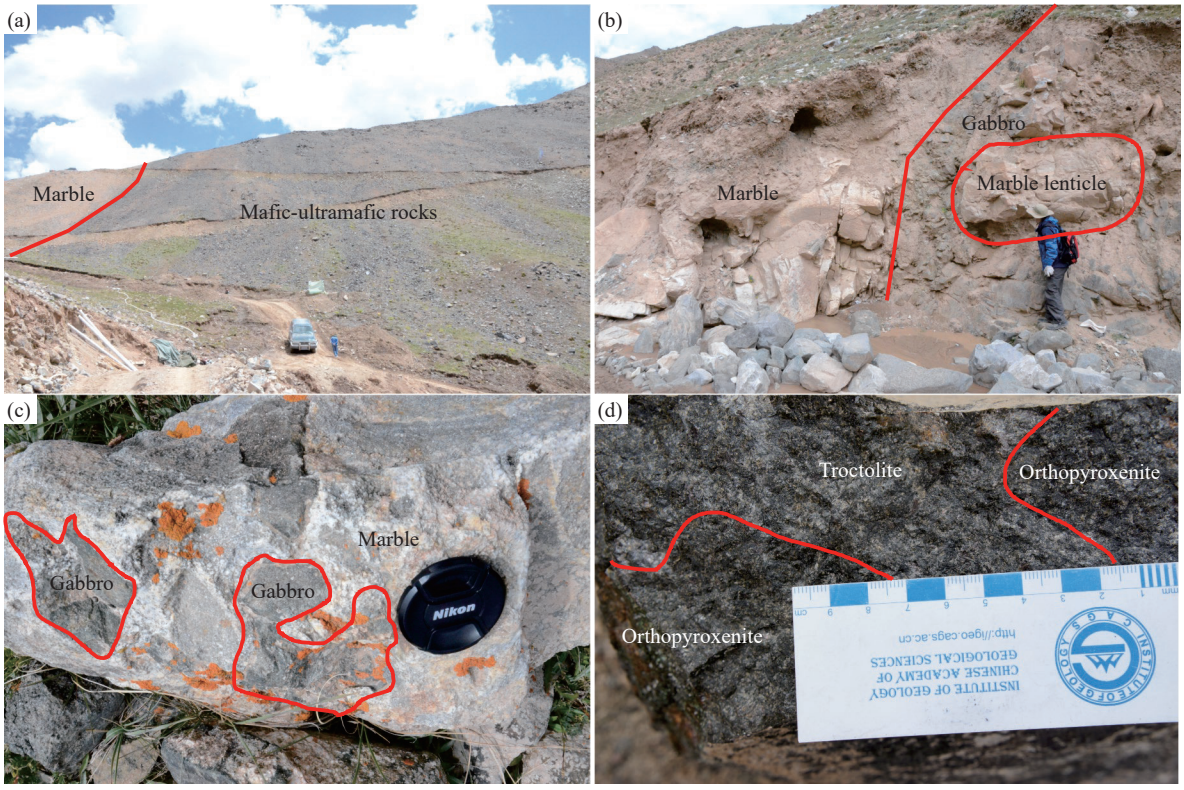

Fig. 3. Outcrop of the STKD intrusion. a–outcrop of mafic-ultramafic rocks; b–intrusive contact relationship between mafic-ultramafic rocks and marble Outcrop of mafic-ultramafic rocks; c–intrusive irregular shape gabbro rocks in marble of Jinshuikou Group; d–gradational relationship between orthopyroxenite and troctolite.

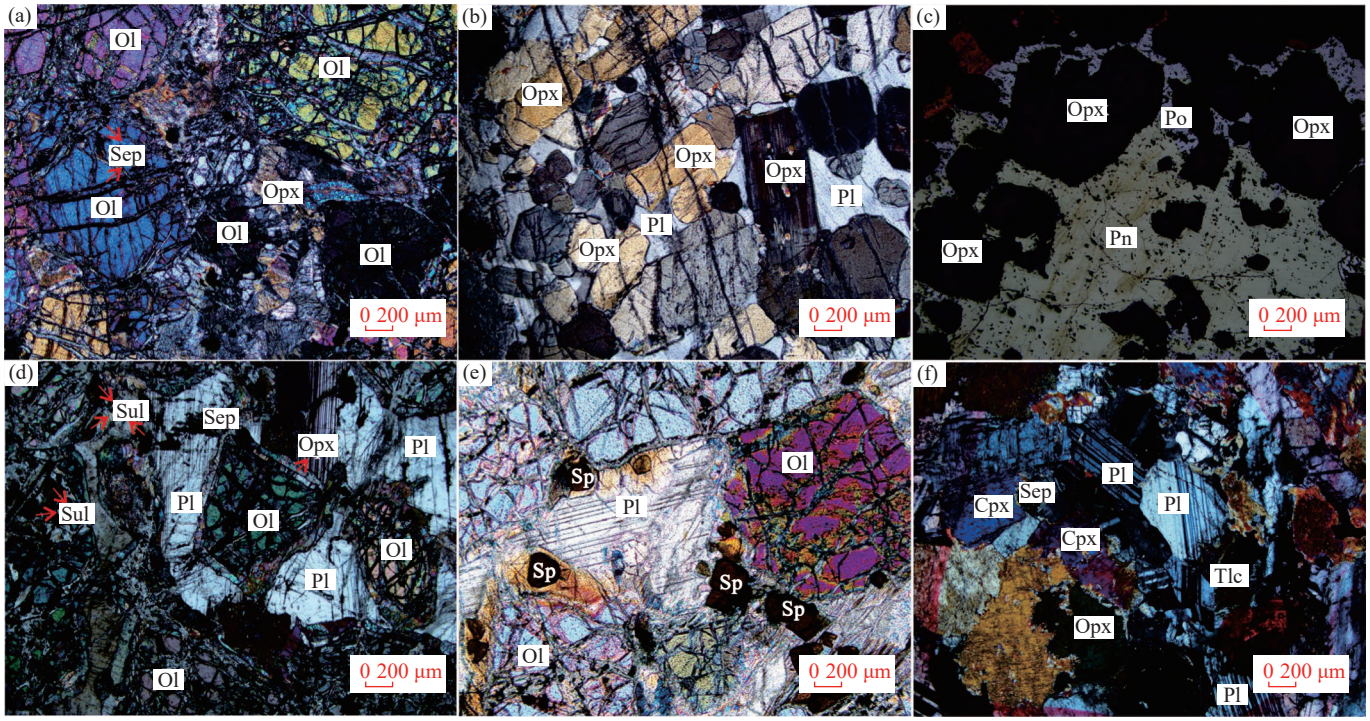

Fig. 4. Microphotographs of mafic-ultramafic rocks and ores in the STKD intrusion. a–cumulus olivine with stockwork serpentine and intercumulus plagioclase in harzburgite, crossed polars; b–cumulus pyroxene and intercumulus plagioclase in plagioclase-bearing orthopyroxenite, crossed polars; c–sideronitic texture. Irregular pyrrhotite and pentlandite fill between orthopyroxene particles, reflecting light; d–orthopyroxene zonal texture of olivine and speckled sulfides in troctolite, crossed polars; e–euhedral spinel and olivine with stockwork serpentine in troctolite, crossed polars; f–euhedral pyroxene alteration in gabbro (serpentinization and talcose), crossed polars; Pl–Plagioclas; Ol–Olivine; Opx–Orthopyroxene; Cpx–Clinopyroxene; Sp–Spinel; Sep–Serpentine; Tlc–Talc; Sul–Sulfide; Po–Pyrrhotite; Pn–Pentlandite.

4.2. Zircon LA-ICP-MS U-Pb dating and Hf isotope

Flotation and electromagnetic methods were used to separate zircon grains for U-Pb dating in the laboratory at the Regional Geology Survey in Langfang City, Hebei Province, China. The large zircon grains with no visible microfractures and clean smooth surfaces were collected using a binocular microscope, mounted in an epoxy resin button and then polished to expose the approximate mid-grain interior. Zircons were observed in transmitted light photomicrographs and cathodoluminescence (CL) images (Fig. 5) were used to select proper crystals for analysis.

The concentrations and isotope compositions of U, Th and Pb were measured by an MC-ICP-MS (Neptune, Thermo Fisher Scientific, Germany) coupled to an (ESI) UP193FX ArF Excimer laser ablation system with 193nm wavelength at the Tianjin Institute of Geology and Mineral Resources, China. The laser pulse rate of 8–10 Hz with an energy density of approximately 13–14 J/cm^2 was selected to produce an ablation pit ranging in diameter 35 μm. During laser ablation, helium was applied as a carrier gas and argon was used as the make-up gas, which enhance the transport efficiency of the ablated material. Details of the instrument were described by Yuan SD et al. (2011). Zircon NIST612 was used as an external standard for U-Th-Pb concentrations analysis. Fractionation correction of the U-Pb isotope was conducted using TEMORA as an external standard (Li HK et al., 2009). Off-line raw data selection and integration of background and analyte signals were reduced using the ICP-MS Data Cal (Liu YS et al., 2010) and Isoplot programs (Ludwig KR, 2003).

Based on the U-Pb dating and cathodoluminescence (CL) images, the Hf isotope analyses of zircons were performed using a Neptune multi-collector ICP-MS (Thermo Fisher Scientific, Germany) equipped with New Wave UP 213 at the Institute of Mineral Resources, Chinese Academy of Geological Sciences, Beijing. A stationary spot with a beam diameter of 35 μm was used as a carrier gas to transport the ablated sample from the laser-ablation cell to the ICP-MS torch via a mixing chamber mixed with Ar. The operating conditions and the analytical procedures were described in detail by Wu FY et al. (2006) and Hou KJ et al. (2007).

The $^{176}Lu/^{175}Lu$=0.02658 and $^{176}Yb/^{173}Yb$=0.796218 ratios were determined to correct for isobaric interferences of ^{176}Lu and ^{176}Yb on ^{176}Hf. For instrumental mass bias correction, Yb isotope ratios were normalized to $^{172}Yb/^{173}Yb$ of 1.35274 and the Hf isotope ratios to $^{179}Hf/^{177}Hf$ of 0.7325, using an exponential law. Zircon sample GJ 1 was used as a reference standard, with a weighted mean $^{176}Hf/^{177}Hf$ ratio of 0.282008±19 (2σ, n=10) during routine analyses. The offline processing of analytical data was performed using the ICP-MSDataCal program (Liu YS et al., 2010).

4.3. Whole-rock major and trace elements

Major whole-rock analyses were analyzed by wet chemical techniques on a wavelength X-ray fluorescence spectrometer (3080E) at the National Research Center of

Geoanalysis, Chinese Academy of Geological Sciences (CAGS). Trace and rare earth elements (REEs) were analyzed using an inductively coupled plasma-mass spectrometer (ICP-MS, X-series) at the same laboratory. The analytical deviations of trace elements and REEs were less than 5% and those of major elements were less than 1%.

5. Analytical results

5.1. Mineral chemistry

Minerals in STKD rocks mainly comprise of olivine, pyroxene and spinel. Mineral chemical compositions of STKD mafic-ultramafic rocks are listed in Appendix Tables 1–3.

Olivine is one of the major rock-forming minerals of the STKD intrusion, and is particularly abundant in mineralized horizons. The olivine crystals are chrysolite with the forsterite contents (Fo) ranging from 82–90. The NiO contents of olivine grains vary from high-Mg (Fo_{89}) in harzburgite to Fo_{82} in troctolite. Olivine Ni contents lower than 2200×10^{-6}, varying between 503×10^{-6} to 1697×10^{-6}, are propitious to mineralization. Compared to XRHM (Ni contents 1564×10^{-6}–2687×10^{-6}), olivine in STKD has lower Ni contents related to the same Fo values.

Spinel contains Cr_2O_3 (28.3–29.7%), Al_2O_3(36.6–38.0%), MgO (11.9–12.8%), FeO(19.7–21.1%). Compared to XRHM (Cr#=46–52, Mg#=40–46, respectively), spinel in STKD has low Cr# (33–35) and high Mg# (50–54).

Clinopyroxene is present in most samples. Clinopyroxene is intercumulus subhedral olivine grains and plagioclase in olivine-bearing varieties. Clinopyroxene is mainly diopside with En=45–47, Wo=46–49, Fs=4.3–5.6.

Orthopyroxene is respectively with En=81–84 in orthopyroxenite, En=83–90 in Harzburgite and En=82–83 in troctolite. Mg# of orthopyroxenes increases from troctolites (85–86) to orthopyroxenites (86–88) to harzburgites (88–91).

5.2. Geochronology

One fresh troctolite sample (K14-7-2.1) obtained from the outcrop at 35°56′54″N，96°11′19″E was dated. The zircon grains are translucent, typically 60–120 μm in length and with a length/width ratio from 1.5 to 2. The CL images show that the interior of the grains is either structurally homogeneous or develops an apparent oscillating zonation. The zircons contain U (91×10^{-6}–791×10^{-6}) and Th (11×10^{-6}–336×10^{-6}) and have Th/U ratios of 0.12–0.78, implying a magmatic origin.

Nineteen analytical spots analyzed by LA-ICP-MS are listed in Appendix Table 4. Most of the zircons produce concordant U-Pb ages (Fig. 6), and yield a weighted mean $^{206}Pb/^{238}U$ age of 412±5 Ma (MSWD=3.2). This age is interpreted as the crystallization age of the STKD troctolite, indicating that the rocks were formed in the Early Devonian and are within the error of the age of the XRHM intrusion.

5.3. Geochemical characteristics

Nine fresh samples, including three harzburgites, two

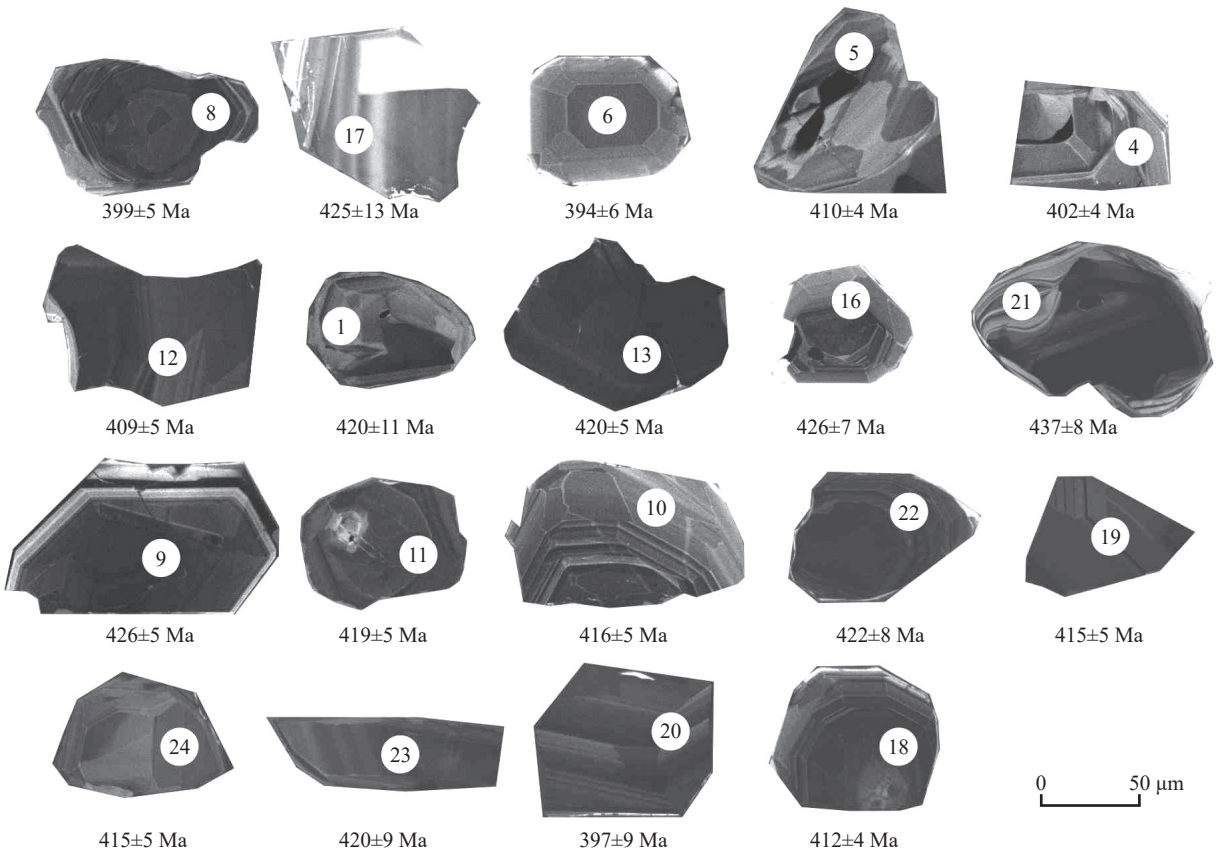

Fig. 5. CL images of zircons from troctolite in the STKD intrusion.

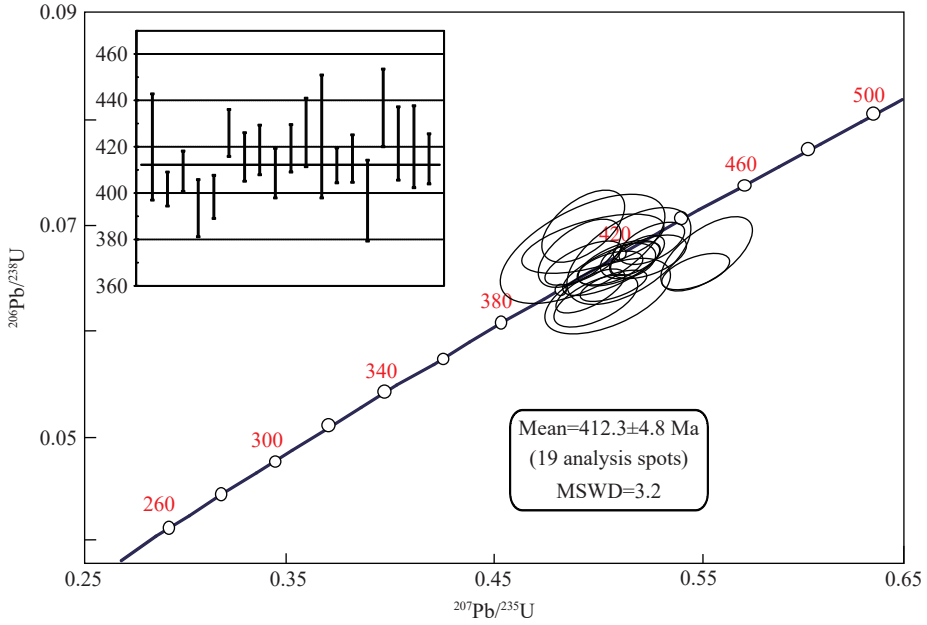

Fig. 6. Zircons U-Pb concordia diagram and weighted average ages diagram for troctolite.

orthopyroxenites, Ol-gabbros and troctolites, respectively, were selected for major and trace element analyses.

5.3.1. Major elements

Whole-rock major and trace element analysis results are shown in Appendix Table 5. The samples contain 38.38%–51.11% SiO_2, are characterized by low TiO_2 contents (0.09%–0.99%) and alkali (Na_2O+K_2O) contents (0.17%–1.30%), but exhibit wide variations in MgO, Al_2O_3, CaO and TFe_2O_3 contents (14.89%–39.62%, 2.26%–13.55%, 1.72%–18.39% and 5.18%–12.18%, respectively). The samples have $Mg^{\#}$ = 81.8–88.1 (mean of 85.3) and the m/f $Mg^{2+}/(TFe^{2+}+Mn^{2+})$ values in the range 4.4–7.3 (mean of 5.8), belonging to the range of ferrous-ultramafic rocks (2.0–6.5) and benefited to the formation of Ni-Cu sulfide mineralization (Wu LR, 1963).

The harzburgites are low in SiO_2 (38.37%–38.61%), CaO (1.72%–2.75%) and Al_2O_3 (2.26%–3.21%), but high in MgO (36.72%–39.62%) and TFe_2O_3(11.31%–12.18%). The orthopyroxenite has high SiO_2, CaO and Al_2O_3 contents (45.55%–51.05%, 3.12%–5.25%, 4.54%–7.84%, respectively) and low MgO and TFe_2O_3 contents (24.59%–28.60%, 10.80%–11.22%, respectively). Ol-gabbro samples reveal a range of the major element contents, SiO_2 (50.33%–51.11%), CaO (18.02%–18.39%), Al_2O_3 (7.20%–7.63%) and MgO (14.89%–15.82%), reflecting their high contents of plagioclase and clinopyroxene. Troctolite samples reveal a relatively large range of the CaO (13.72%–17.04%) and Al_2O_3 (10.04%–13.55%) contents, whereas contents of SiO_2 (44.05%–51.11%) and MgO (14.89%–19.58%) are in a narrow range. Samples are plotted in the mafic-ultramafic cumulate area in the AFM diagram (Fig. 7a), indicating their cumulative origin. From peridotites to gabbros show tholeiite series to calc-alkalic series in the SiO_2-TFeO/MgO diagram (Fig. 7b). The whole-rock compositions are normalized to 100% based on an LOI- and sulfide-free basis.

5.3.2. Trace elements

Trace element concentrations from STKD mafic-ultramafic samples are listed in Table S5. The chondrite-normalized trace element patterns of the rocks are broadly sub-parallel (Fig. 8a). The rocks have relatively low REEs concentrations with a total content of the rare-earth element (ΣREE) ranging from 4.21×10^{-6}–39.73×10^{-6}. Most values of the samples for LREE/HREE of 1.59–2.98, La_N/Yb_N of 0.83–2.60, La_N/Sm_N of 0.84–2.17, Gd_N/Yb_N of 1.86–2.33 indicate weak fractionation between LREE and HREE. Ultramafic rock samples are characterized by slight enrichment of REE compared to the heavy REE and by a slight δEu positive anomaly (1.08–1.30). Gabbro samples (including troctolites and Ol-gabbros) show nearly flat chondrite-normalized REE patterns with a slight δEu negative anomaly (0.79–1.01), which differs from gabbro sample data with significant δEu positive anomaly from Jia LH et al. (2021).

The samples of harzburgite and orthopyroxenite are highly enriched in LILEs (Rb, Sr and Th) and depleted in Nb and Ta compared to Th and La on primitive-mantle-normalized spidergrams (Fig. 8b). Gabbro samples are also characterized by a pronounced negative Nb and Ta anomaly and LILEs enrichment (e.g., Th). The REE and trace element patterns from STKD are in accord with patterns of XRHM mafic-ultramafic rocks that have been reported, suggesting a common origin.

5.3.3. Hf isotopes of zircon

The Lu-Hf isotope compositions of 21 zircon grains from the troctolite sample are listed in Appendix Table 6. The $^{176}Yb/^{177}Hf$ values range from 0.004680 to 0.019360 and the $^{176}Lu/^{177}Hf$ values from 0.000256 to 0.000894. The $^{176}Hf/^{177}Hf$ values are between 0.282549 and 0.282767. Twenty-one spots correspond to positive $\varepsilon Hf_{(t)}$ values ranging from 1.1 to 8.6 with a weighted average of 4.5, yielding

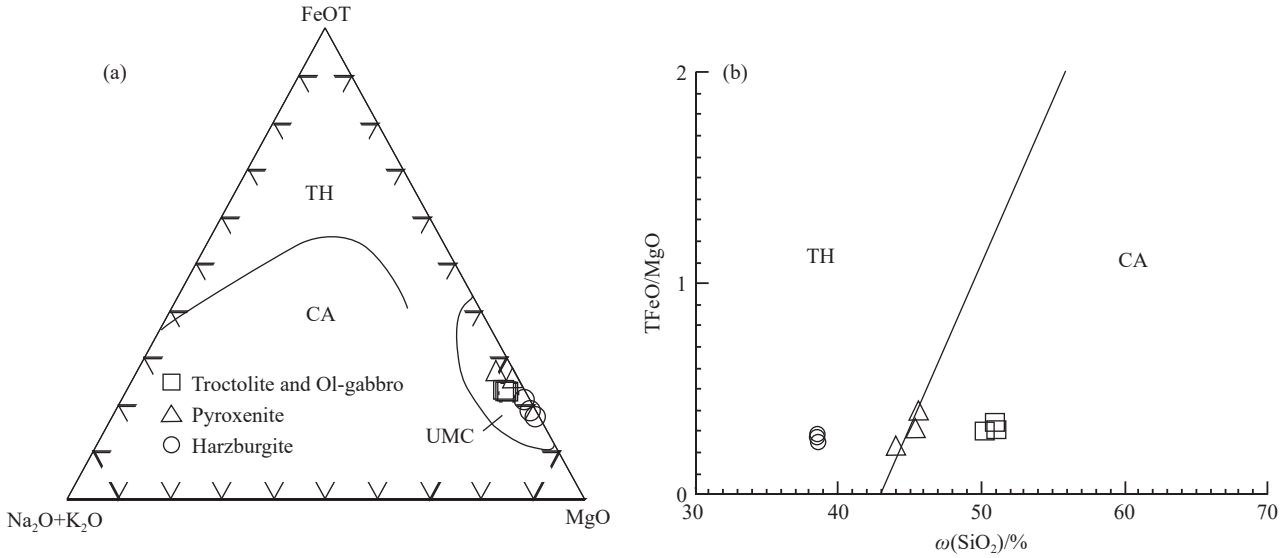

Fig. 7. a–AFM diagram of STKD intrusion (Coleman RG, 1977); b–SiO_2-TFeO/MgO diagram of STKD intrusion (Miyashiro A, 1974). TH–tholeiite series; CA–calc-alkalic series; UMC–Ultramafic rocks

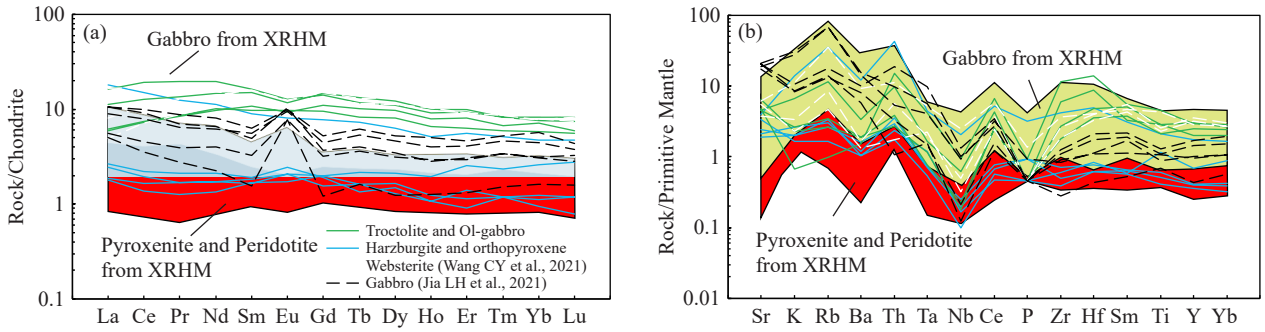

Fig. 8. a–Chondrite-normalized REE patterns of the STKD intrusion; b–primitive mantle-normalized element spider diagram of the STKD intrusion (The primitive mantle and chondrite data are from Sun SS and McDonough WF (1989). Data of gabbro, pyroxenite and peridotite from XRHM (XRHM) are from Wang G et al.(2014) and Jiang CY et al.(2015).

$^{176}Lu/^{177}Hf$ values of less than 0.002. The calculated zircon model ages (t_{DM1}) range from 686–976 Ma.

6. Discussion

6.1. Magmatic events in STKD intrusion

The age of mafic-ultramafic rocks in the Eastern Kunlun are listed in Table 1. Zircon U-Pb ages of mafic-ultramafic rocks from STKD intrusion indicate two major episodes of magmatism: early episode of the gabbro (425 Ma, Zhang ZW et al., 2018a), the olivine websterite (420 Ma, Jia LH et al., 2021) and troctolite (412 Ma), and the late episode of the olivine websterite (334 Ma, Zhang ZW et al., 2018b). The gabbro from the early episode is coeval with 427 Ma ore-barren gabbro at XRHM (Wang G et al., 2014; Peng B et al., 2016). The olivine websterite and troctolite with ages of 410 Ma are similar to the ore-bearing ultramafic rocks at XRHM (Song XY et al., 2016). Recently, some distinct hydrothermal Pb-Zn ore bodies have been found in the XRHM mining area, and their hydrothermal titanite and apatite have U-Pb ages of 414–413 Ma (Chen X et al., 2023). The development of magmatic and hydrothermal metallogenic systems in the XRHM mining area are interrelated both in time and space, indicating the coexistence of magmatic and hydrothermal ore-forming systems, promoting comprehensive prospecting evaluation (Chen X et al., 2023). The late episode is consistent with zircon U-Pb ages of Buqingshan basalts (340 Ma, Bian QT et al., 1999) and gabbro (333 Ma, Liu ZQ et al., 2011).

6.2. Contamination and fractional crystallization

Crustal contamination provides critical information for magmatic sulfide deposits, which are possibly critical for both metal and sulfur sources (Mavrogenes JA et al., 1999; Ripley EM et al., 1999; Li CS et al., 2001; Holzhied A et al., 2002). Hf isotope data from both STKD and XRHM intrusion diagram between the Hf isotopic evolution lines of chondrite and depleted mantle, closer to the depleted mantle line, indicating a potential contaminant (Fig. 9). Ore-bearing intrusion is commonly assimilated by country rocks in the STKD intrusion. Although the boundary between the intrusion and country rocks is not very clear in some sections (Fig. 3c), gradual transits to each other can be observed. The

Table 1. Age of mafic-ultramafic rocks in the Eastern Kunlun.

Number	Location	Lithofacies	Methods	Age/Ma	References
1	Buqingshan	Ophiolite	LA-ICP-MS	436	Ren JH et al., 2009
2	Xiarihamu	Gabbro	LA-ICP-MS	431.3±2.1	Li CS et al., 2015
3	Binggounan	Gabbro	LA-MC-ICP-MS	427.5±7.1	Wang BZ et al., 2014
4	Shuitoukengde	Gabbro	SHRIMP	424.7±3.7	Zhang ZW et al., 2018b
5	Akechukesai	Pyroxenite	LA-ICP-MS	422±10	Yan JM, 2017
6	Detangou	Gabbro	LA-ICP-MS	413.4±0.8	Yan JM et al., 2018
7	Xiarihamu	Websterite	SHRIMP	411.6±2.4	Li CS et al., 2015
8	Yuejinshan	Gabbro	LA-ICP-MS	406±3.0	Liu B et al., 2012
9	Xiwanggou	Ore-bearing	LA-ICP-MS	406.9±3.0	Kong HL et al., 2019
10	Xiarihamu	Websterite	SHRIMP	406.1±2.7	Song XY et al., 2016
11	Xiarihamu	Gabbronorite	SHRIMP	405.5±2.7	Song XY et al., 2016
12	Xiangyanggou	Gabbro	LA-ICP-MS	398.8±1.8	Yan JM et al., 2018
13	Binggounan	Olivine-pyroxenite	SHRIMP	377.8±3.4	Zhang ZW et al., 2017
14	Shuitoukengde	Olivine	SHRIMP	333.9±4.2	Zhang ZW et al., 2018b
15	Xiaojiashan	Gabbro	LA-ICP-MS	247.1±1.1	Wang YL et al., 2017
16	Xiaojiashan	Gabbro	LA-MC-ICP-MS	227.8±0.9	Ao C et al., 2015
17	Kaimuqi	Websterite	LA-ICP-MS	221.0±2.3	Liu YG et al., 2019
18	Langmuri	Gabbro, Olivine pyroxenolite	LA-ICP-MS	440-430	Li L et al., 2022

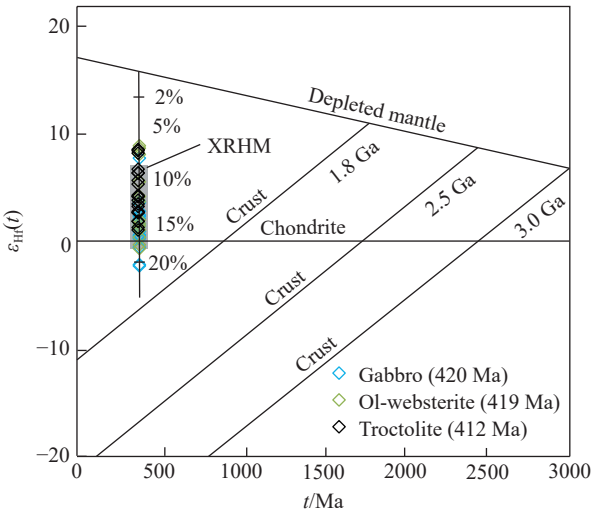

Fig. 9. Zircon Hf isotopic features for gabbro in STKD intrusion. Gabbro and Ol-websterite data are from Jia LH et al. (2021). XRHM (Xiarihmau) mafic-ultramafic rocks data are from Wang G et al. (2014) and Jiang CY et al. (2015).

assimilation and contamination processes, which took place mantle-derived magma during ascent, may lead to the increase of SiO_2 and LILEs and the decrease of HFSEs abundance. Samples of STKD mafic-ultramafic rocks show the relative enrichment of LILEs (Rb, Th, U, K) and relatively depleted in HFSEs (Nb and Ta) and the La/Yb, Ce/Yb, Th/Yb, Nb/La and La/Sm values suggest the limited crustal contamination during the rise of the magma.

Ultramafic rocks comprising olivine with <Fo_{90}, >0.1% CaO and <0.3% NiO are generally interpreted to be related to the fractional crystallization of primitive magmas and of not mantle origin (Pál-Molnár E et al., 2015). The olivine crystals are chrysolite with a forsterite content (Fo) ranging from 81–86, obviously lower than mantle origin olivine, indicating the processes of fractionation and crystallization. Meanwhile, according to the distribution coefficient of Mg-Fe between olivine and melts (0.3–0.33, Ross JR and Tarvis GA, 1981), the primary magma MgO content can be calculated using the olivine with the highest Fo value. Using the olivine with Fo value of 88.9, the primary magma of STKD intrusion belongs to high MgO basaltic magma containing about 11.7% MgO, suggesting the intrusion is derived from 11.2%–14.0% partial melting of the mantle. Due to the rebalancing between the early-crystalline olivine and the residual inter-crystalline melt, the MgO content would be lower than that of the olivine crystallized from the primary magma. Thus, the actual MgO content is slightly more than 11.7%. Combine with the fact that the spinel in STKD has low Cr# (33.3–35.3) and high Mg# (50.4–53.9), indicating the low degrees of partial melting (Dick HJB et al., 1984).

The role played by assimilation and contamination can be accurately identified by using the correlations and changes between trace elements ratios with similar partition coefficients (e.g. Ce/Pb, Th/Yb), as the ratios are not affected by the degree of fractional crystallization and partial melting (Campbell IH and Griffiths RW, 1993). The distribution coefficients of Nb/U and Ce/Pb remain constant during partial melting and magmatic differentiation, therefore their values are indicative of their origin. The samples show a close correlation between La/Yb-Ce/Yb and Th/Yb-Nb/La (Figs. 10a, b), different to the weak correlation between Zr/Nb-Th/Nb and Nb/Ce-Nb/U (Figs. 10c, d), indicating the degree of crustal contamination is limited. The samples have relatively low La/Sm ratios of 0.85–3.11 to high La/Sm ratios (>4.5) which generally represent crustal contamination, indicating limited crustal contamination. In addition, the Ce/Pb ratio of STKD rocks ranges from 0.25 to 16.03, which is obviously lower than the typical mantle ratio of 25±5 (Hofmann AW, 1997); Nb/U ratio varys from 0.64 to 2.40 that is similar to the values of the continental crust but differs from that of MORB and OIB (47±10; Hofmann AW, 1997), suggesting contamination crustal rather than towards a mantle origin. Primitive mantle-normalized trace element patterns are

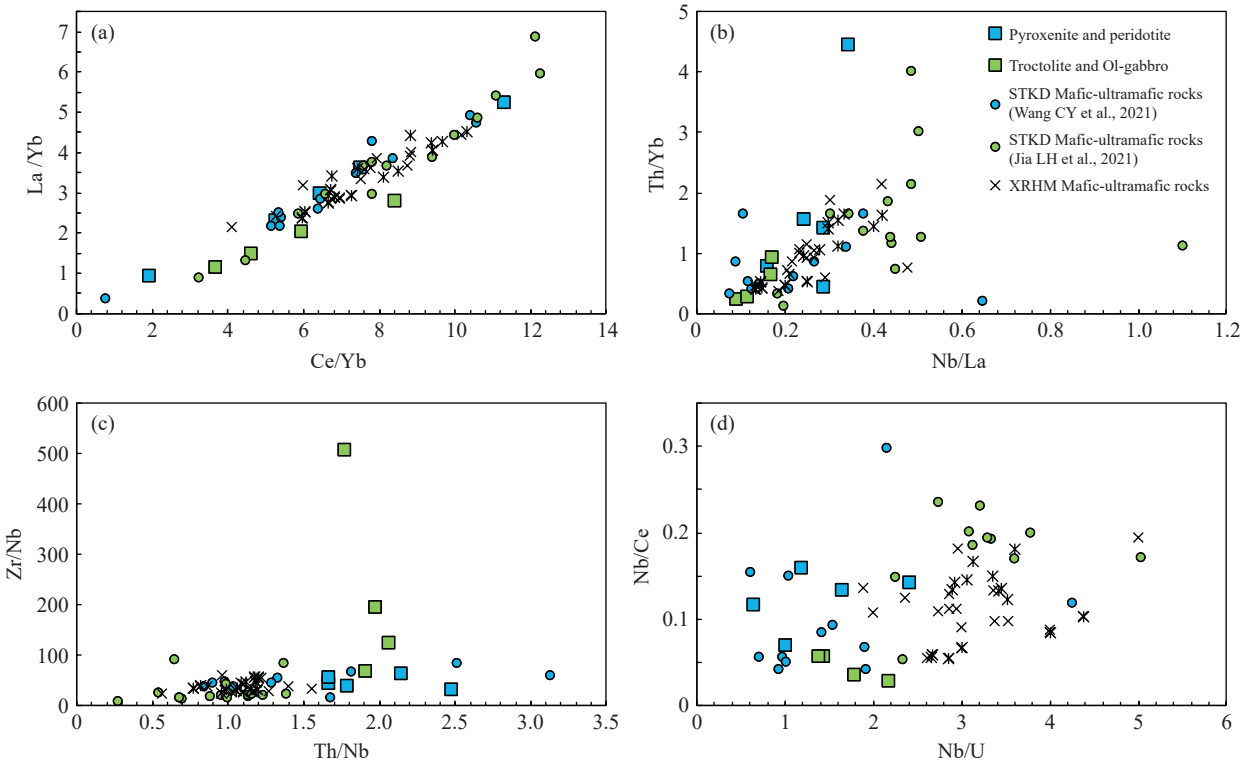

Fig. 10. Plots of selected trace elements for checking contamination of STKD intrusion. XRHM mafic-ultramafic rocks data are from Wang G et al. (2014) and Jiang CY et al. (2015).

characterized by the enrichment of LILEs, positive anomalies of HFSEs, and negative anomalies of Nb and Ta. In addition, the regional anomalies of higher LILEs/HFSEs ratios compared with MORB, chondrite-normalized LREE enrichment and flat HREE patterns, may be responsible for crustal contamination. The contamination of SiO_2 and S from biotite-plagioclase gneisses may lead to the sulfide saturation in STKD (Jia LH et al., 2021; Wang CY et al., 2021).

6.3. Magma sources

Compared to the primitive mantle, average crust and lower crust, the samples have relatively low Nb/La (0.08–0.34, avg. 0.21) and Nb/Ce (0.03–0.16, avg. 0.09) ratios, indicating the HFSEs reflect the characteristics of magma sources. The enrichment of LILEs and HFSEs of the STKD intrusion may reflect the mantle metasomatism, which is caused by the influx of slab-released fluids and/or melts, may be resulted from the partial melting of the subducted slab. In Nb/Yb-Th/Yb diagram (Fig. 11a), the samples all deviate from the MORB-OIB evolution line and are close to the volcanic arc array, due to the influence of subduction components (Pearce JA et al., 1995). In addition, Ba/Th, Th/Nb ratios are useful for identifying an aqueous fluid and a subduction zone sediment component. In the Ba/Th *vs.* Th/Nb discrimination diagram (Figs. 11b, c), the samples have an addition of slab fluid trend, indicating that the mantle source was metasomatized by subduction-related fluids. In conclusion, based on the above analyses, the parental magmas of the STKD intrusion were derived from fluid-metasomatized depleted lithosphere mantle sources.

All zircon ε_{Hf} values of the troctolite from STKD intrusion are plotted in the range between chondrite and depleted mantle evolution trend lines (Fig. 9), which suggests the parental magma was derived from a depleted source mantle and experienced contamination during ascent. The Hf isotopic compositions of zircons from STKD intrusion all have positive $\varepsilon_{Hf}(t)$ values varying from 1.1 to 8.6 that is similar to the depleted mantle, suggesting the intrusion derived from a mantle source with a higher Lu/Hf ratio than chondrite. Although Precambrian gneiss is widely exposed at the STKD ore district, their Hf isotope compositions are currently unavailable. Compared with the zircon $\varepsilon_{Hf}(t)$ values of Precambrian gneiss that represents a potential crustal composition in the Qaidam orogenic belt at Dulan (Xiong Q et al., 2012), our data show that 5–15% contamination maybe occur to parental magma. The middle positive $\varepsilon_{Hf}(t)$ values suggest that the mantle source of the magma had undergone melting due to source mixing, and the Hf isotopic reservoir of the mantle is dominant. The mixing source may have the characteristic of depleted mantle Hf isotopic compositions or enriched mantle Hf isotopic compositions. It depends on the proportion of the crustal material in the magma (Zheng YF et al., 2007). The zircon originated from a differential source of depleted mantle relative to chondrite based on Hf isotopic data between the Hf isotope evolution lines of chondrite and depleted mantle in Figure 9. The Hf model ages of the zircons derived directly from the unmodified mantle may reflect the time when they separated from the depleted mantle (Vervoort JD and Kemp AIS, 2016). A comparison of zircon model ages (t_{DM1}) with that of the XRHM ultramafic rocks, both

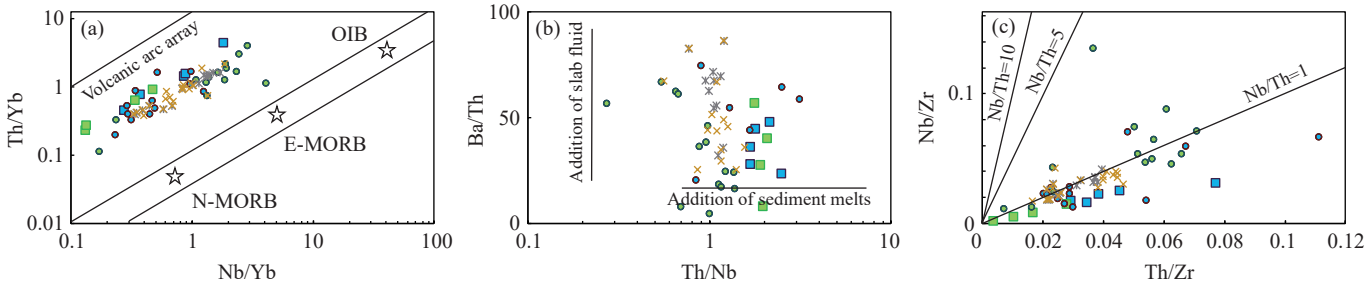

Fig. 11. Nb/Yb *vs.* Th/Yb(a), Th/Nb *vs.* Ba/Th(b), Th/Zr *vs.* Nb/Zr(c) diagrams of the STKD intrusion (a after Pearce JA, 2008; b after Hanyu T et al., 2006; c after Woodhead JD et al., 2001). The legends and data sources are consistent with Fig. 9.

significantly older than their crystallization ages (610–875 Ma, Wang G et al., 2014). The Hf model age is older than the magmatic crystallization age of STKD intrusion, suggesting that the magma has undergone degrees of enrichment (Wu et al., 2007).

6.4. Tectonic setting

The available data show that the initial subduction of the Proto-Tethys ocean in the EKO occurred before the Pre-Cambrian (Yang JS et al., 1996; Feng JY et al., 2010). Large volumes of igneous rocks, such as Yaziquan arc diorite with an age of 480 Ma (Cui MH et al., 2011) and arc-related basaltic-dacitic lava with an age of 448 Ma (Chen NS et al., 2002), were associated with the northward subduction of the Proto-Tethyan oceanic plate. Hornblende diabases of the Huxiaoqin mafic rocks with a magmatic crystallization age of 438 Ma in the Central Kunlun Suture Zone may suggest the end of Early Paleozoic ocean subduction (Liu B et al., 2013b). By ca.430–420 Ma, the discovery of the continental-type eclogite (428 Ma) constrains the timing of the closure of the Proto-Tethys orogeny with the eclogite-facies metamorphism at 428 Ma (Meng FC et al., 2013b). Then, voluminous post-collision magma and Ni-Co-(Cu)-bearing magma were generated during the late Silurian-Early Devonian (427–410 Ma). Meanwhile, extensional tectonic regimes generated extensive A-type granites and S-type granites and gabbros with ages of 424–393 Ma (Liu B et al., 2012; Liu B et al., 2013a; Xiong FH et al., 2013). Recently, 420–409 Ma bimodal volcanics are supposed to be formed in the post-collisional extensional setting, and represent that EKOB evolved into a post-collisional collapse stage since Late Silurian (Li RB et al., 2020). Generally, the end of Proto-Tethys orogeny in the EKOB is marked by the molasse sediments (423–400 Ma) (Lu L et al., 2010).

The zircon $^{206}Pb/^{238}U$ age of 412 Ma indicates that the STKD troctolite formed in the Early Devonian, similar to the XRHM ore-bearing ultramafic rocks (Zhang ZW et al., 2015; Song XY et al., 2016), implying the extensive Late Silurian and Early Devonian magmatism occurred in the East Kunlun. The geochemistry characteristics suggest the metasomatism of the mantle sources of the STKD intrusion was probably related to the subduction of the Proto-Tethys Ocean crust. XRHM mafic-ultramafic rocks are considered to be Alaskan-type intrusions in the orogenic belts (Li CS et al., 2015). Alaskan-type intrusions are characterized by cumulus textures, occurrence of abundant clinopyroxene (rich in CaO) and water-bearing minerals such as hornblende and biotite (rich in fluid), and the scarcity of orthopyroxene (Irvine TN, 1974). The rock-forming minerals of STKD intrusion are olivines, orthopyroxenes, clinopyroxenes and plagioclases, different to the classic Alaskan-type rocks. These features suggest that the STKD intrusion may not be the Alaskan-type intrusion. The enrichment of LILEs and depletion of HFSEs may reflect the metasomatism of mantle sources by the influx of slab-released fluids derived from the partial melting of the subducted slab as mentioned earlier. Magma formed in a post-collisional environment may have island arc geochemical signatures (Aldanmaz E et al., 2000; Wang KL et al., 2004b). Therefore, the source region may retain properties of previously subducted oceanic crust, such as the enrichment in LILEs and depletions in HFSEs. Meanwhile, a post-collisional extension setting already existed in the early Devonian according to regional research data, leading to the formation of mafic-ultramafic intrusive and Ni-Co-(Cu) sulfide mineralization.

In conclusion, the STKD Ni-Cu sulfide-mineralized intrusion was formed in a post-collisional extensional setting, which is similar to XRHM Ni-Cu sulfide deposit that located in the western part of East Kunlun.

6.5. Metallogenetic potentiality

Although there are several early Devonian mafic-ultramafic intrusions in EKOB, such as Xiangyanggou (399 Ma, Yan JM et al., 2018), Detangou (413 Ma, Yan JM et al., 2018), Binggounan (Wang G et al., 2014), Akechukesai (422 Ma, Yan JM, 2017) there is no significant metallogenic signature. In order to summarize regional Ni-Co-(Cu) metallogenic regulation, we compared STKD to XRHM Ni-Co deposit and Langmuri ore occurrence (Table 2). These three are consistent with rock-type and rock-forming ages, indicating similar tectonic setting. EKOB may have potential economic Ni-Cu sulfide-ore body, and the mafic-ultramafic intrusions from the same tectonic setting may be an important direction for further exploration. By comparing the characteristics of ore-bearing rock between the XRHM deposit and STKD ore occurrence, it is found that the country rock of XRHM ore-bearing rocks is mainly silica-rich gneisses, while the country rock of STKD intrusion is mainly

Table 2. Comparison of mineralization geological features from Xiarihamu, Shitoukengde and Langmuri Ni-Co ore occurrence in East Kunlun.

Deposit Name	Xiarihamu	Shitoukengde	Langmuri
Host Rock	Harzburgite, orthopyroxenite	Ehrwaldite, olivine gabbro, troctolite	Serpentinized dunite
Associated Rocks	Meso- and Neoproterozoic Jinshuikou Group gneisses, marble and amphibolite	Meso- and Neoproterozoic Jinshuikou Group gneisses, marble and amphibolite	Meso- and Neoproterozoic Jinshuikou Group gneisses, marble and amphibolite
Age	Sulfide Re-Os 410 Ma,gabbro 439–426 Ma,websterite 411 Ma	Gabbro 423 Ma, 426 Ma; olivine websterite 334 Ma	Gabro and olivine orthopyroxenite 440–430 Ma
Ni grade/%	0.69	0.27	0.25
Cu grade/%	0.165	-	-
Co grade/%	0.024	0.02	0.02
Spinel Mg#	40–46	50–54	-
Spinel Cr#	46–52	33–35	-
Olivine Fo	85–87	82–89	
Olivine Ni /$\times10^{-6}$	1564–2687	503–1697	
Orthopyroxene En	84–87	82–90	
Plagioclase An	56–67	67–79	
Whole rock m/f	2.34–6.67	3.83–6.27	1.03–7.81

marble, resulting in obvious differences in mineral assemblage. The main country rocks in the west of XRHM intrusion are silica-rich gneisses, which mainly form massive and sideronitic texture ore, while the main country rocks in the east of XRHM intrusion are calcium-rich marble, which has poor mineralization and forms disseminated ores (Song XY et al., 2016), reflecting that different country rocks may have an influence on mineralization. The XRHM rocks is mainly composed of a large number of orthopyroxenes, forming the main ore-bearing rock types of harzburgite and orthopyroxenite. The main ore-bearing rock types of STKD are still the harzburgite and orthopyroxenite, but the intrusion is mainly composed of olivine-clinopyroxenite, ehrwaldite and troctolite. Ni is one of the most indicative elements for ore-bearing properties in olivine (Barnes SJ et al., 2023), which has higher concentrations in the high-Mg olivine grains. Compared to XRHM (Ni contents 1564×10^{-6}–2687×10^{-6}), Olivine in STKD has lower Ni contents related to the same Fo values, varying between 503×10^{-6} to 1697×10^{-6}, and unfavorable to mineralization. Although STKD intrusion was formed in the similar tectonic setting, a comprehensive evaluation of the rock assemblage is not conducive to the formation of large deposit. The STKD may have the potential to host economic Ni-Cu sulfides but is unable to form super-large deposit like XRHM.

7. Conclusion

(i) Zircon from troctolite at STKD intrusion yielded U-Pb isotope age of 412±5 Ma (MSWD=3.2), which is similar to that of the XRHM mafic-ultramafic ore-bearing rocks.

(ii) Whole-rock elemental and Hf isotopic compositions of the STKD intrusion suggest the parental magma was derived from depleted lithosphere mantle that was metasomatized by subduction-related fluids and experienced limited crustal contamination during ascent.

(iii) STKD intrusion was formed in the post-collisional extensional setting, which making STKD has the potential to host economic Ni-Cu sulfides but unlikely to be a super-large deposit like XRHM.

CRediT authorship contribution statement

Xue-peng Duan conceived of the presented idea, and took the lead in writing the manuscript, Fan-cong Meng provide the original data, Zong-qi Wang and Xiao-fei Yu supervised the finding of this work. All authors discussed the results and contributed to the final manuscript.

Declaration of competing interest

The authors declare no conflicts of interest.

Acknowledgements

Hui-bin Feng, Li-hui Jia, Guang-kuo Tian and Qiang Liu are thanked for their assistance during the field trip. The authors are grateful to the Regional Geology Survey for zircon separation in Langfang City, Hebei Province, China, the Tianjin Institute of Geology and Mineral Resources for LA-ICP-analyses, China. This study is financially supported by the National Natural Science Foundation of China (41272052), and the projects (1212011120158 and 12120114080101) of the China Geological Survey.

Supplementary dataset

Supplementary data (Tables. S1–S5) to this article can be found online at doi: 10.31035/cg2023070.

References

Aldanmaz E, Pearce JA, Thirlwall MF, Mitchell JG. 2000. Petrogenetic

evolution of late Cenozoic, post-collision volcanism in western Anatolia, Turkey. Journal of Volcanology and Geothermal Research, 102, 67–95. doi: 10.1016/S0377–0273(00)00182–7.

Ao C, Sun FS, Li B, Wang G, Li L, Li S, Zhao JW. 2015. U-Pb dating, geochemistry and tectonic implications of Xiaojianshan gabbro in Qimantage Mountain, Eastern Kunlun orogenic belt. Geotectonica Et Metallogenia, 39(6), 1176–1184 (in Chinese with English abstract). doi: 10.16539/j.ddgzyckx.2015.06.016.

Barnes SJ, Yao ZS, Mao YJ, Jesus AP, Yang S, Taranovic V and Maier WD. 2023. Nickel in olivine as an exploration indicator for magmatic Ni-Cu sulfide deposits: A data review and re-evaluation. American Mineralogist, 108(1), 1–17. doi: 10.2138/am-2022-8327.

Bian QT, Li DH, Pospelov I, Yin LM, Li HS, Zhao DS, Chang CF, Luo XQ, Gao SL, Astrakhantsev O. 2004. Age, geochemistry and tectonic setting of Buqingshan ophiolites, North Qinghai-Tibet Plateau, China. Journal of Asian Earth Sciences, 23(4), 577–596. doi: 10.1016/j.jseaes.2003.09.003.

Bian QT, Luo XQ, Li HS, Chen HH, Zhao DS. Li DH. 1999. Discovery of Early Paleozoic and Early Carboniferous-Early Permian ophiolites in the A'nyemaqen, Qinghai province, China. Scientia Geologica Sinica, 34(3), 437–438 (in Chinese with English abstract).

Campbell IH, Griffiths RW. 1993. The evolution of the mantle`s chemical structure. Lithos, 30(3–4), 389–399. doi: 10.1016/0024-4937(93)90047-G.

Chai G, Naldrett AJ. 1992. Charicteristics of Ni-Cu-PGE Mineralization and genesis of the Jinchuan deposit, Northwest China. Economic Geology, 87, 1475–1495. doi: 10.2113/gsecongeo.87.6.1475.

Chen LM, Song XY, Hu RZ, Yu SY, Yi JN, Kang J, Huang KJ. 2021. Mg-Sr-Nd isotopic insights into petrogenesis of the Xiarihamu Mafic-Ultramafic Intrusion, Northern Tibetan Plateau, China. Journal of Petrology, 62(2), egaa113. doi: 10.1093/petrology/egaa113.

Chen NS, Li XY, Zhang KX, Wang GC, Zhu YH, Hou GJ, Bai YS. 2006. Lithological characteristics of the Baishahe Formation to the south of Xiangride town, Eastern Kunlun Mountains and its age constrained. Geological Science and Technology Information, 25, 1–7 (in Chinese with English abstract). doi: 10.1007/s11442-006-0415-5.

Chen NS, Sun M, He L, Zhang KX, Wang GC. 2002. Precise timing of the Early Paleozoic metamorphism and thrust deformation in the Eastern Kunlun Orogen. Chinese Science Bulletin, 47(13), 1130–1133 (in Chinese with English abstract). doi: 10.1360/02tb9253.

Chen NS, Sun M, Wang QY, Zhao GC, Chen Q, Shu GM. 2007. EMP chemical ages of monazites from Central Zone of the eastern Kunlun Orogen: Records of multi-tectonometamorphic events. Chinese Science Bulletin, 52(16), 2252–2263 (in Chinese with English abstract). doi: 10.1007/s11434-007-0299-5.

Chen X, Wang H, Mao JW, Yu M, Qiao JF, Wang ZA. 2023. Genesis and geological significance of hydrothermal Pb-Zn orebodies in Xiarihamu mining area, East Kunlun Mountains, China. Earth Science Frontiers, 160(2), 347–369 (in Chinese with English abstract). doi: 10.13745/j.esf.sf.2022.2.76.

Coleman RG, 1977. Ophiolites: Ancient Oceanic Lithosphere? Springer-Verlag, Berlin, Heidelberg, New York, 1–229. doi: 10.1007/978–3–642–66673–5.

Cui MH, Meng FC, Wu XK. 2011. Early Ordovician island arc of Yaziquan, west of Qimantag Mountain, eastern Kunlun: Evidences from geochemistry, Sm-Nd isotope and geochronology of intermediate-basic igneous rocks. Acta Petrologica Sinica, 27(11), 3365–3379 (in Chinese with English abstract). doi: 10.2110/jsr.2011.62.

Dick HJB, Bullen T. 1984. Chromian spinel as a petrogenetic indicator in abyssal and alpine-type peridotites and spatially associated lavas. Contributions to Mineralogy and Petrology, 86(1), 54–76. doi: 10.1007/BF00373711.

Feng JY, Pei XZ, Yu SL, Ding SP, Li RB, Yu S, Zhang YF, Li ZC, Chen YX, Zhang XF. 2010. The discovery of the mafic-ultramafic melange in Kekesha area of Dulan County, East Kunlun region, and its LA-ICP-MS zircon U-Pb age. Geology in China, 37(1), 28–38 (in Chinese with English abstract).

Hanyu T, Tatsumi Y, Nakai S, Chang Q, Miyazaki T, Sato K, Tani K, Shibata T, Yoshida T. 2006. Contribution of slab melting and slab dehydration to magmatism in the NE Japan arc for the last 25 Myr: Constraints from geochemistry. Geochemistry, Geophysics, Geosystems, 7(8), 1–29. doi: 10.1029/2005gc001220.

He DF, Dong YP, Liu XM, Yang Z, Sun SS, Cheng B, Li W. 2015. Tectono-thermal events in East Kunlun, Northern Tibetan Plateau: Evidence from zircon U-Pb geochronology. Gondwana Research, 30, 179–190. doi: 10.1016/j.gr.2015.08.002.

He HL, Chen LM, Song XY, Fu B, Yi JN, Yu SY, Deng YF. 2022. Genesis of the Xiarihamu Magmatic Ni-Co Sulfide Deposit in the East Kunlun Orogen, Northern Tibetan Plateau: In Situ Oxygen Isotope and Geochemical Perspectives. Economic Geology. doi: 10.5382/econgeo.4949.

Hofmann AW. 1997. Mantle geochemistry: the message from oceanic volcanism. Nature, 385, 219–229. doi: 10.1038/385219a0.

Holzhied A, Grove TL. 2002. Sulfur saturation limits in silicate melts and their implications for core formation scenarios for terrestrial planets. American Mineralogist, 87(2−3), 227–237. doi: 10.2138/am–2002–2–304.

Hou KJ, Li YH, Zou TR, Qu XM, Shi YR, Xie GQ. 2007. Laser ablation-MC-ICP-MS technique for Hf isotope microanalysis of zircon and its geological applications. Acta Petrologica Sinica, 23(10), 2595–2604 (in Chinese with English abstract).

Huang H, Niu YL, Nowell G, Zhao ZD, Yu XH, Zhu DC, Mo XX, Ding S. 2014. Geochemical constraints on the petrogenesis of granitoids in the East Kunlun Orogenic belt, northern Tibetan Plateau: Implications for continental crust growth through syn-collisional felsic magmatism. Chemical Geology, 370, 1–18. doi: 10.1016/j.chemgeo.2014.01.010.

Irvine TN. 1974. Petrology of the Duke Island Ultramafic Complex Southeastern Alaska. Geological Society of America Memoirs, 138, 1–244. doi: 10.1130/MEM138–p1.

Jia LH, Mao JW, Li BL, Zhang DY, Sun TT. 2021. Geochronology and petrogenesis of the Late Silurian Shitoukengde mafic–ultramafic intrusion, NW China: Implications for the tectonic setting and magmatic Ni-Cu mineralization in the East Kunlun Orogenic Belt. International Geology Review, 63(5), 549–570. doi: 10.1080/00206814.2020.1722969.

Jiang CF, Yang JS, Feng BG, Zhu ZZ, Zhao M, Chai YC, Shi XD, Wang HD, Hu JQ. 1992. Opening-Closing Tectonics of Kunlun Mountains, Geological Publishing House, Beijing, 1–224 (in Chinese).

Jiang CY, Ling JL, Zhou W, Du W, Wang ZX, Fan YZ, Song YF, Song ZB. 2015. Petrogenesis of the Xiarihamu Ni-bearing layerd mafic-ultramafic in trusion, East Kunlun: Implications for its extensional island arc environment. Acta Geologica Sinica, 31(4), 1117–1136 (in Chinese with English abstract).

Kong HL, Li JC, Guo XZ, Yao XG. Jia QZ. 2019. The discovery of Early Devonian pyroxene peridotite from the Xiwangmu magmatic Ni-Cu sulfide ore spot in East Kunlun Mountains. Geology in China, 46(1), 205–206 (in Chinese with English abstract). doi: 10.12029/gc20190114.

Li CS, Naldrett AJ, Ripley EM. 2001. Critical factors for the formation of a nickel-copper deposit in an evolved magma system: Lessons from comparison of the Pants Lake and Voisey`s Bay sulfide occurrences in Labrador, Canada. Mineralium Deposita, 36, 85–92. doi: 10.1007/s001260050288.

Li CS, Zhang ZW, Li WY, Wang YL, Sun T, Ripley EM. 2015. Geochronology, petrology and Hf-S isotope geochemistry of the

newly-discovered Xiarihamu magmatic Ni-Cu sulfide deposit in the Qinghai-Tibet plateau, western China. Lithos, 216–217, 224–240. doi: 10.1016/j.lithos.2015.01.003.

Li HK, Geng JZ, Hao S, Zhang YQ, Li HM. 2009. The study of zircon U–Pb dating by means LA-MC-ICPMS. Bulletin of Mineralogy, Petrology and Geochemistry, 29(s1), 600–601 (in Chinese with English abstract). doi: 10.16461/j.cnki.1000-4734.2009.s1.014600.

Li L, Sun FY, Li SJ, Li BL, Qian H, Wang C, Zhao TF, Yu L, Wang G, Huo L, Wang L, Zhang YJ, Wang LL, Li HR, Yan JM, Li YJ, Zhang DX, Yang YQ, Wang W. 2022. Metallogenic geological conditions and regularity of magmatic Cu-Ni sulfide deposits in the East Kunlun metallogenic belt. Journal of Jilin University (Earth Science Edition), 52(5), 1461–1496 (in Chinese with English abstract). doi: 10.13278/j.cnki.jjuese.20220045.

Li RB, Pei XZ, Li ZC, Patias D, Su ZG, Pei L, Chen GC, Chen YX, Liu CJ. 2020. Late Silurian to Early Devonian volcanics in the East Kunlun orogen, northern Tibetan Plateau: Record of postcollisional magmatism related to the evolution of the Proto-Tethys Ocean. Journal of Geodynamics, 140, 101780. doi: 10.1016/j.jog.2020.101780.

Li RB, Pei XZ, Wei B, Li ZC, Pei L, Chen GC, Chen YX, Liu CJ. 2021. Middle Cambrian-Early Ordovician ophiolites in the central fault of the East Kunlun Orogen: Implications for an epicontinental setting related to Proto-Tethyan Ocean subduction. Gondwana Research, 94, 243–258. doi: 10.1016/j.gr.2021.02.017.

Li RB, Pei XZ, Wei B, Li ZC, Pei L, Chen YX, Liu CJ, Cheng GC, Wang M, Feng K. 2019. Constraints of late Cambrian mafic rocks from the Qushi'ang ophiolite on a back-arc system in a continental margin, East Kunlun Orogen, Western China. Journal of Asian Earth Sciences, 169, 117–129. doi: 10.1016/j.jseaes.2018.08.006.

Li WY, Zhang ZW, Gao YB, Chen B, Hong J. 2021. Tectonic transformation the Kunlun orogen of Paleo-Tethys, North China, and the metallization of critical mineral resource 's nickel, cobalt, manganese and lithium. Geology in China, 49(5), 1385–1407 (in Chinese with English abstract). doi: 10.12029/gc20220503.

Li WY, Zhang ZW, Wang YL, Zhang JW, You MX, Zhang ZB, Norbu N. 2022. Tectonic transformation of proto- and Paleo-Tethys and the metallization of magmatic Ni-Cu-Co sulfide deposits in Kunlun Orogen, Northwest China. Journa of Earth Sciences and Environment, 44(1), 1–19 (in Chinese with English abstract). doi: 10.19814/j.jese.2021.08033.

Liu B, Ma CQ, Guo P, Zhang JY, Xiong FH, Huang J, Jiang HA. 2013a. Discovery of the middle Devonian A-type granite from the Eastern Kunlun Orogen and its tectonic implications. Earth Science - Journal of China University of Geosciences, 38(5), 947–962 (in Chinese with English abstract). doi: 10.3799/dqkx.2013.093.

Liu B, Ma CQ, Jiang HA, Guo P, Zhang JY, Xiong FH. 2013b. Early Paleozoic tectonic transition from ocean subduction to collisional orogeny in the Eastern Kunlun region: Evidence from Huxiaoqin mafic rocks. Acta Petrologica Sinica, 29(6), 2093–2106 (in Chinese with English abstract). doi: 10.2113/gssajg.116.1.169.

Liu B, Ma CQ, Zhang JY, Xiong FH, Huang J, Jiang HA. 2012. Petrogenesis of Early Devonian intrusive rocks in the east part of Eastern Kunlun Orogen and implication for Early Palaeozoic orogenic processes. Acta Petrologica Sinica, 28(6), 1785–1807 (in Chinese with English abstract).

Liu Q, Meng FC, Li SR, Feng HB, Jia LH, Tian GK. 2016. Geochronology of zircon from the paragneiss of Kuhai Group in southern East Kunlun terrane. Acta Petrologica Et Mineralogica, 35(3), 469–483 (in Chinese with English abstract).

Liu YG, Chen ZG, Li WY, Xu XH, Kou X, Jia QZ, Zhang ZW, Liu F, Wang YL, You MX. 2019. The Cu-Ni mineralization potential of the Kaimuqi mafic-ultramafic complex and the indicators for the magmatic Cu-Ni sulfide deposit exploration in the East Kunlun Orogenic Belt, Northern Qinghai-Tibet Plateau, China. Journal of Geochemical Exploration, 198, 41–53. doi: 10.1016/j.gexplo.2018.12.002.

Liu YG, Li WY, Jia QZ, Zhang ZW, Wang ZA, Zhang ZB, Zhang JW, Qian B. 2018. The dynamic sulfide saturation process and a possible Slab Break-off Model for the giant Xiarihamu Magmatic Nickel Ore Deposit in the East Kunlun Orogenic Belt, Northern Qinghai-Tibet Plateau, China. Economic Geology, 113(6), 1383–1417. doi: 10.5382/econgeo.2018.4596.

Liu YJ, Genser J, Neubauer F, Jin W, Ge XH, Handler R, Takasu A. 2005. $^{40}Ar/^{39}Ar$ mineral ages from basement rocks in the Eastern Kunlun Mountains, NW China, and their tectonic implications. Tectonophysics, 398(3−4), 199–224. doi: 10.1016/j.tecto.2005.02.007.

Liu YS, Gao S, Hu ZC, Gao CG, Zong KQ, Wang DB. 2010. Continental and oceanic crust recycling-induced melt-peridotite interactions in the Trans-North China Orogen: U-Pb dating, Hf isotopes and trace elements in zircons from mantle xenoliths. Journal of Petrology, 51, 537–571. doi: 10.1093/petrology/egp082.

Liu ZQ, Pei XZ, Li RB, Li ZC, Zhang XF, Liu ZG, Chen GC, Chen YX, Ding SP. 2011. LA-ICP-MS zircon U-Pb geochronology of the two suites of ophiolites at the Buqingshan Area of the A'nyemaqen Orogenic Belt in the Southern Margin of East Kunlun and its tectonic implication. Acta Geologica Sinica. 85 (2), 185–194 (in Chinese with English abstract). doi: CNKI:SUN:DZXE.0.2011-02-005.

Lu L, Wu ZH, Hu DG, Barosh JP, Hao S, Zhou CJ. 2010. Zircon U-Pb ages for rhyolite of the Maoniushan Formation and its tectonic significance in the east Kunlun Mountains. Acta Petrologica Sinica, 26(4), 1150–1158 (in Chinese with English abstract).

Ludwig KR. 2003. Users Manual For Isoplot 3.00: A Geochronological Toolkit for Microsoft Excel. Berkeley Geochronological Center Special Publication No, 25–32.

Ma CQ, Xiong FH, Yin S, Wang LX, Gao K. 2015. Intensity and cyclicity of orogenic magmatism: An example from a Paleo-Tethyan granitoid batholith, Eastern Kunlun, northern Qinghai-Tibetan Plateau. Acta Petrologica Sinica, 31(12), 3555–3568 (in Chinese with English abstract).

Mavrogenes JA, O 'Neill HSC. 1999. The relative effects of pressure, temperature and oxygen fugacity on the solubility of sulfide in mafic magmas. Geochimica et Cosmochimica Acta, 63(7-8), 1173–1180. doi: 10.1016/s0016–7037(98)00289–0.

Meng FC, Cui MH, Jia LH, Ren YF, Feng HB. 2015a. Paleozoic continental collision of the East Kunlun orogen: Evidence from protoliths of the eclogites. Acta Petrologica Sinica, 31(12), 3581–3594 (in Chinese with English abstract).

Meng FC, Cui MH, Wu XK, Ren YF. 2015b. Heishan mafic–ultramafic rocks in the Qimantag area of Eastern Kunlun, NW China: Remnants of an Early Paleozoic incipient island arc. Gondwana Research, 27(2), 745–759. doi: 10.1016/j.gr.2013.09.023.

Meng FC, Cui MH, Wu XK, Wu JF, Wang JF. 2013a. Magmatic and metamorphic events recorded in granitic gneisses form the Qimantag, East Kunlun Mountains, Northwest China. Acta Petrologica Sinica, 29(6), 2107–2122 (in Chinese with English abstract).

Meng FC, Zhang JX, Cui MH. 2013b. Discovery of Early Paleozoic eclogite from the East Kunlun, Western China and its tectonic significance. Gondwana Research, 23, 825–836. doi: 10.1016/j.gr.2012.06.007.

Miyashiro A. 1974. Volcanic rock series in island arcs and active continental margins. American Journal of Science, 274(4), 321–355. doi: 10.2475/ajs.274.4.321.

Mo XX, Luo ZH, Deng JF, Yu XH, Liu CD, Chen HW, Yuan WM, Liu YH. 2007. Granitoids and crustal growth in the east Kunlun orogenic belt. Geological Journal of China University, 13(3), 403–414 (in Chinese with English abstract). doi: 10.16108/j.issn1006-7493.2007.03.004.

Naldrett AJ. 1997. Key factors in the genesis of Noril'sk, Sudbury, Jinchuan, Voisey's Bay and other world-class Ni-Cu-PGE deposits: Implications for exploration. Australian Journal of Earth Sciences, 44(3), 283–315. doi: 10.1080/08120099708728314.

Pál-Molnár E, Batki A, Almási E, Kiss B, Upton BGJ, Markl G, Odling N, Harangi S. 2015. Origin of mafic and ultramafic cumulates from the Ditrău Alkaline Massif, Romania. Lithos, 239, 1–18. doi: 10.1016/j.lithos.2015.09.022.

Pan YS, Zhou WM, Xu RM, Wang DA, Zhang YQ, Xie YW, Chen TG, Luo H. 1996. Geological characteristics and evolution of the Kunlun Mountains region during the early Paleozoic. Science in China Ser D, 39(4), 337–347.

Pearce JA. 2008. Geochemical fingerprinting of oceanic basalts with applications to ophiolite classification and the search for Archean oceanic crust. Lithos, 100(1-4), 14–48. doi: 10.1016/j.lithos.2007.06.016.

Pearce JA, Peate DW. 1995. Tectonic Implications of the Composition of Volcanic Arc Magmas. Annual Review of Earth and Planetary Sciences, 23(1), 251–285. doi: 10.1146/annurev.ea.23.050195.001343.

Peng B, Sun FY, Li BL, Wang G, Li SJ, Zhao TF, Li L, Zhi YB. 2016. The geochemistry and geochronology of the Xiarihamu II mafic–ultramafic complex, Eastern Kunlun, Qinghai Province, China: Implications for the genesis of magmatic Ni–Cu sulfide deposits. Ore Geology Reviews, 73, 13–28. doi: 10.1016/j.oregeorev.2015.10.014.

Ren JH, Liu YQ, Qiao F, Han WZ. 2009. LA-ICP-MS U-Pb zircon dating and geochemical characteristics of diabase-dykes from the Qingshuiquan area, eastern Kunlun orogenic belt. Acta Petrologica Sinica, 25(5), 1135–1145 (in Chinese with English abstract).

Ripley EM, Park YR, Li CS, Naldrett AJ. 1999. Sulfur and oxygen isotopic evidence of country rock contamination in the Voisey`s Bay Ni-Cu-Co deposit, Labrador, Canada. Lithos, 47, 53–68. doi: 10.1016/S0024–4937(99)00007–9.

Ross JR and Travis GA. 1981. The nickel sulfide deposits of Western Australia in global perspective. Economic Geology, 76(6), 1291–1329. doi: 10.2113/gsecongeo.76.6.1291.

Shao FL, Niu YL, Liu Y, Chen S, Kong JJ, Duan M. 2017. Petrogenesis of Triassic granitoids in the East Kunlun Orogenic Belt, northern Tibetan Plateau and their tectonic implications. Lithos, 282–283, 33–44. doi: 10.1016/j.lithos.2017.03.002.

Song XY, Wang KY, Barnes SJ, Yi JN, Chen LM, Schoneveld LE. 2020. Petrogenetic insights from chromite in ultramafic cumulates of the Xiarihamu intrusion, northern Tibet Plateau, China. American Mineralogist, 105(4), 479–497. doi: 10.2138/am–2020–7222.

Song XY, Yi JN, Chen LM, She YW, Liu CZ, Dang XY, Yang QA, Wu SK. 2016. The giant Xiarihamu Ni-Co sulfide deposit in the East Kunlun Orogenic Belt, Northern Tibet Plateau, China. Economic Geology, 111, 29–55. doi: 10.2113/econgeo.111.1.29.

Sun SS, McDonough WF. 1989. Chemical and isotopic systematics of oceanic basalts; Implications for mantle composition and processes. Geological Society London Special Publications, 42(1), 313–345. doi: 10.1144/GSL.SP.1989.042.01.19.

Vervoort JD, Kemp AIS. 2016. Clarifying the zircon Hf isotope record of crust–mantle evolution. Chemical Geology, 425, 65–75. doi: 10.1016/j.chemgeo.2016.01.023.

Wang BZ, Jing C, Luo ZH, Chen FB, Tao W, Guo GE. 2014. Spatial and temporal distribution of Late Permian-Early Jurassic intrusion assemblages in eastern Qimantag, East Kunlun, and their tectonic settings. Acta Petrologica Sinica, 30(11), 3213–3228 (in Chinese with English abstract).

Wang CY, Zhang ZW, Zhang CJ, Chen CH, Li Y, Qian B. 2021. Constraints on sulfide saturation by crustal contamination in the Shitoukengde Cu-Ni deposit, East Kunlun orogenic belt, northern Qinghai-Tibet Plateau, China. Geosciences Journal, 25(3), 401–415. doi: 10.1007/s12303–020–0025–8.

Wang G, Sun FY, Li BL, Li SJ, Zhao JW, Ao C, Yang QA. 2014. Zircon U-Pb geochronology and geochemistry of the mafic-ultramafic intrusion in Xiarihamu Cu-Ni deposit from East Kunlun, with implications for geodynamic setting. Earth Science Frontiers (China University of Geosciences (Beijing); Peking University), 21(6), 381–401 (in Chinese with English abstract). doi: 10.13745/j.esf.2014.06.036.

Wang GC, Chen NS, Zhu YH, Zhang KX. 2003. Late Caledonian Ductile Thrusting Deformation in the Central East Kunlun Belt, Qinghai, China and its significance: evidence from geochronology. Acta Geologica Sinica, 77(3), 311–319 (in Chinese with English abstract). doi: 10.1111/j.1755-6724.2003.tb00747.x.

Wang GC, Wang QH, Jian P, Zhu YH. 2004a. Zircon SHRIMP ages of Precambrian metamorphic basement rocks and their tectonic significance in the eastern Kunlun Mountains, Qinghai Province, China. Earth Science Frontiers, 11, 481–490 (in Chinese with English abstract). doi: 10.1007/BF02873097.

Wang GC, Wei QR, Jia CX, Zhang KX, Li DW, Zhu YH, Xiang SY. 2007. Some ideas of Precambrian Geology in the East Kunlun, China. Geological Bulletin of China, 26, 929–937 (in Chinese with English abstract). doi: 10.3969/j.issn.1671-2552.2007.08.003.

Wang KL, Chung SL, O'Relly SY, Sun SS, Shinjo R, Chen CH. 2004b. Geochemical Constraints for the Genesis of Post-collisional Magmatism and the Geodynamic Evolution of the Northern Taiwan Region. Journal of Petrology, 45(5), 975–1011. doi: 10.1093/petrology/egh001.

Wang YL, Zhang ZW, Zhang JW, Qian B, Liu YG, You MX. 2017. Early Mesozoic mantle-derived magmatic events and their geological significance in the East Kunlun orogenic belt. Geology & Exploration, 53(5), 855–866 (in Chinese with English abstract). doi: 10.13712/j.cnki.dzykt.2017.05.003.

Wang YS, Chen JN. 1987. Metamorphic Zone and Metamorphism in Qinghai Province and its Adjacent Areas. Geological Publishing House, Beijing, 1–248 (in Chinese).

Wei B, Wang CY, Li CS and Sun YL. 2013. Origin of PGE-Depleted Ni-Cu sulfide mineralization in the Triassic Hongqiling No. 7 orthopyroxenite intrusion, Central Asian Orogenic Belt, Northeastern China. Economic Geology, 108(8), 1813–1831. doi: 10.2113/econgeo.108.8.1813.

Woodhead JD, Hergt JM, Davidson JP, Eggins SM. 2001. Hafnium isotope evidence for 'conservative' element mobility during subduction zone processes. Earth and Planetary Science Letters, 192, 331–346. doi: 10.1016/S0012–821X(01)00453–8.

Wu FY, Li XH, Zheng YF, Gao S. 2007. Lu-Hf isotopic systematics and their applications in petrology. Acta Petrologica Sinica, 23(2), 185–220 (in Chinese with English abstract). doi: 10.3321/j.issn:1000-0569.2007.02.001.

Wu FY, Yang YH, Xie LW, Yang JH, Xu P. 2006. Hf isotopic compositions of the standard zircons and baddeleyites used in U-Pb geochronology. Chemical Geology, 234(1–2), 105–126. doi: 10.1016/j.chemgeo.2006.05.003.

Wu GJ, Xiao XC, Li TD. 1989. The Yadong-Golmud geoscience section on the Qinghai-Tibet plateau. Acta Geological Sinica, 63, 285–296 (in Chinese with English abstract). doi: 10.19762/j.cnki.dizhixuebao.1989.04.001.

Wu LR. 1963. Metallogenic specialization of mafic-ultramafic rocks of China. Scientia Geologica Sinica, 1, 29–41.

Xia R, Deng J, Qing M, Li WL, Guo XD, Zeng GZ. 2017. Petrogenesis of ca. 240 Ma intermediate and felsic intrusions in the Nan'getan: Implications for crust–mantle interaction and geodynamic process of the East Kunlun Orogen. Ore Geology Reviews, 90, 1099–1117. doi: 10.1016/j.oregeorev.2017.04.002.

Xie W, Song XY, Deng YF, Wang YS, Ba DH, Zheng WQ, Li XB. 2012. Geochemistry and petrogenetic implications of a Late Devonian mafic–ultramafic intrusion at the southern margin of the Central Asian Orogenic Belt. Lithos, 144–145, 209–230. doi: 10.1016/j.lithos.2012.03.010.

Xiong FH, Ma CQ, Jiang HA, Liu B, Huang J. 2013. Geochronology and geochemistry of Middle Devonian mafic dykes in the East Kunlun orogenic belt, Northern Tibet Plateau: Implications for the transition from Prototethys to Paleotethys orogeny. Chemie der Erde-Geochemistry, 74(2), 225–235. doi: 10.1016/j.chemer.2013.07.004.

Xiong Q, Zheng JP, Griffin WL, O'Reilly SY, Pearson NJ. 2012. Decoupling of U-Pb and Lu-Hf isotopes and trace elements in zircon from the UHP North Qaidam orogen, NE Tibet (China): Tracing the deep subduction of continental blocks. Lithos, 155, 125–145. doi: 10.1016/j.lithos.2012.08.022.

Xu ZQ, Yang JS, Jiang M, Li HB, Xue GQ, Yuan XC, Qian H. 2001. Deep structure and lithospheric shear faults in the East Kunlun-Qiangtang region, northern Tibetan Plateau. Science in China. Series D, Earth Sciences, 1–9. doi: 10.1007/BF02911965.

Xu ZQ, Yang JS, Li HB, Yao JX. 2006. The Early Palaeozoic terrene framework and the formation of the High-Pressure (HP) and Ultra-High Pressure (UHP) Metamorphic Belts at the Central Orogenic Belt (COB). Acta Geologica Sinica, 80(12), 1793–1806 (in Chinese with English abstract). doi: 10.1111/j.1745-4557.2006.00081.x.

Xu ZQ, Yang JS, Li HB, Zhang JX, Wu CL. 2007. Orogenic Plateau: Terrane Amalgamation, Collision and Uplift in the Qinghai-Tibet Plateau, Geological Publishing House, Beijing, 1–458 (in Chinese).

Yan JM, Sun FY, Li L, Yang YQ, Zhang DX. 2018. A slab break-off model for mafic–ultramafic igneous complexes in the East Kunlun Orogenic Belt, northern Tibet: insights from early Palaeozoic accretion related to post-collisional magmatism. International Geology Review, 1–18. doi: 10.1080/00206814.2018.1501618.

Yan JM. 2017. Study on Geological Characteristics and Genesis of Akechukesai Copper-Nickel Deposit in East kunlun, Qinghai Province. Changchun, Jilin University, Master Thesis, 1–63 (in Chinese with English abstract).

Yang HH, Wang Q, Li YB, Lin B, Song Y, Wang YY, He W, Li HW, Li S, Li JL, Liu CC, Feng SB, Xin T, Fu XL, Liang XJ, Zhang Q, Wang BQ, Li Y. 2022. Geology and mineralization of the Tiegelongnan supergiant porphyry-epithermal Cu (Au, Ag) deposit (10 Mt) in western Tibet, China: A review. China Geology, 5(1), 136–159. doi: 10.31035/cg2022001.

Yang JS, Robinson PT, Jiang CF, Xu ZQ. 1996. Ophiolites of the Kunlun Mountains, China and their tectonic implications. Tectonophysics, 258(1–4), 215–231. doi: 10.1016/0040–1951(95)00199–9.

Yuan SD, Peng JT, Hao S, Li HM, Geng JZ, Zhang DL. 2011. In situ LA-MC-ICP-MS and ID-TIMS U-Pb geochronology of cassiterite in the giant Furong tin deposit, Hunan Province, South China: New constraints on the timing of tin–polymetallic mineralization. Ore Geology Reviews, 43(1), 235–242. doi: 10.1016/j.oregeorev.2011.08.002.

Zhang JX, Yu SY, Li YS, Yu XX, Lin YH, Mao XH. 2015. Subduction, accretion and closure of Proto-Tethyan Ocean: Early Paleozoic accretion/collision on oregeny in the Altun-Qilian-North Qaidam orogenic system. Acta Petrologica Sinica, 31(12), 3531–3554 (in Chinese with English abstract).

Zhang YL, Hu DG, Shi YR, Lu L. 2010. SHRIMP zircon U-Pb ages and tectonic significance of Maoniushan Formation volcanic rocks in East Kunlun orogenic belt, China. Geological Bulletin of China, 29(11), 1614–1618 (in Chinese with English abstract). doi: 10.3969/j.issn.1671-2552.2010.11.003.

Zhang ZW, Li WY, Qian B, Wang YL, Li SJ, Liu CZ, Zhang JW, Yang QA, You MX and Wang ZA. 2015. Metallogenic epoch of the Xiarihamu magmatic Ni-Cu sulfide deposit in eastern Kunlun orogenic belt and its prospecting significance. Geology in China, 42(3), 438–451 (in Chinese with English abstract).

Zhang ZW, Wang CY, Qian B, Li WY. 2018a. The geochemistry characteristics of Silurian gabbro in East Kunlun Orogenic Belt and its mineralization relationship with magmatic Ni-Cu sulfide deposit. Acta Petrologica Sinica, 34(8), 2262–2274 (in Chinese with English abstract).

Zhang ZW, Wang YL, Qian, B, Li WY. 2017. Zircon SHRIMP U-Pb age of the Binggounan magmatic Ni-Cu deposit in East Kunlun Mountains and its tectonic implications. Acta Geologica Sinica, 91(4), 724–735 (in Chinese with English abstract). doi: 10.3799/dqkx.2018.588.

Zhang ZW, Wang YL, Qian B, Liu YG, Zhang DY, Lü PR, Dong J. 2018b. Metallogeny and tectonomagmatic setting of Ni-Cu magmatic sulfide mineralization, number I Shitoukengde mafic-ultramafic complex, East Kunlun Orogenic Belt, NW China. Ore Geology Reviews, 96, 236–246. doi: 10.1016/j.oregeorev.2018.04.027.

Zhao ZM, Ma HD, Wang BZ, Bai YS, Li RS, Ji WH. 2008. The evidence of Intrusive Rocks obout Collision-Orogeny during Early Devonian in Eastern Kunlun Area. Geological Review, 54(1), 47–56 (in Chinese with English abstract). doi: 10.16509/j.georeview.2008.01.007.

Zheng YF, Chen RX, Zhang SB, Tang J, Zhao ZF, Wu YB. 2007. Zircon Lu-Hf isotope study of ultrahigh-pressure eclogite and granitic gneiss in the Daie orogen. Acta Petrologica Sinica, 23(2), 317–330 (in Chinese with English abstract).

Zhou W, Wang BY, Xia MZ, Xia ZD, Jiang CY, Dong J, Xie ES. 2016. Mineralogical charocteristics of Shitoukengde mafic-ultramafic intrusion and analysis of its metallogenic potential, East Kunlun. Acta Petrologica Et Mineralogica, 35(1), 81–96 (in Chinese with English abstract). doi: 10.3969/j.issn.1000-6524.2016.01.006.

Zhu YH, Zhang KX, Chen NS, Wang GC, Hou GJ. 1999. Determination of different ophiolitic belts in eastern Kunlun orogenic zone and their tectonic significance. Earth Science-Journal of China University of Geosciences, 24(2), 134–138 (in Chinese with English abstract). doi: 10.3321/j.issn:1000-2383.1999.02.006.